2008

Synthesis And Characterization Of Polymer-derived Porous Sicn Ceramics

Yun Wei

University of Central Florida

SYNTHESIS AND CHARACTERIZATION OF POLYMER-DERIVED POROUS SiCN CERAMICS

by:

YUN WEI

Bachelor, Kunming University of Science and Technology, China 2002

A thesis submitted in partial fulfillment of the requirements
for the degree of Master of Science
in the Department of Mechanical, Materials and Aerospace Engineering
in the College of Engineering and Computer Science
at the University of Central Florida
Orlando, Florida

Fall Term
2008

Major Professor: Linan An

ABSTRACT

The synthesis and characterization of porous SiCN ceramics produced by the method of polymer-derived ceramics were studied in this work. The polymer-to-ceramic conversion technique is a novel revolution in the methods for fabricating porous materials with controlled morphologies and tailored properties. The porous SiCN ceramics can be successfully prepared from thermal decomposition of polymeric precursors (polysilazane) and the pore former (polyvinyl alcohol (PVA)). The fabrication procedures involved the mixing of the pre-ceramic precursor with appropriate concentration of the PVA, curing, pyrolysis and subsequent PVA removal, leaving pores in the ceramic matrix. The material obtained revealed a homogeneous amorphous microstructure consisting of Si, C and N elements.

The effects of the concentration and the particle size of PVA on the bulk density, open porosity, line shrinkage, microstructure, pore size, permeability, mechanical behavior, oxidation behavior and thermal stability were examined in this thesis. An increase in both concentration and particle size of PVA contribute to a decrease in the bulk density and an increase in the open porosity and line shrinkage. The morphology development, in particular, was investigated by scanning electron microscopy (SEM). The properties in terms of the pore

size and permeability were measured by the water expulsion method. The mechanical behavior of the porous SiCN ceramic was characterized by the three- point bending strength test, thermal shock strength test and hertzian indentation strength test. The flexural strength and hertzian indentation strength of these porous ceramics at room temperature decrease with an increase in porosity. However, the flexural strength after thermal shock was significantly improved by increasing the temperature change. The oxidation behavior and thermal stability of porous SiAlCN ceramics were also explored by the mass change versus oxidation time and temperature. The phase evolution at different temperatures was also investigated by XRD analysis.

ACKNOWLEDGMENTS

I greatly appreciate the help of Professor Linan An, my advisor. He encouraged me and gave me great advice during my study and research at UCF. He provided direction for my research so that I can get the results as soon as possible.

I would also like to thank Professor Lei Zhai and Professor Samar Kalita for their assistance with experimental equipments. I also appreciate Dr Ligong Zhang, Dr. Weifeng Fei, Mr Arnold Hill and Mr. Tao Jiang for their support in preparing samples and maintaining apparatus.

I would especially like to thank my family, for their immense love, support, and constant encouragement.

TABLE OF CONTENTS

LIST OF FIGURES

LIST OF TABLES

LIST OF ACRONYMS/ABBREVIATIONS

CVI	Chemical Vapor Infiltration
HIP	Hot Isostatic Pressure
PDC	Polymer-derived Ceramics
PDPC	Polymer-derived Porous Ceramics
PVA	Polyvinyl Alcohol
PU	Polyurethane
RFI	Rigid Fiber Insulation
SEM	Scanning electron microscopy
TGA	Thermogravimetry Analysis
VL20	Ceraset Polysilazane 20
XRD	X-ray Diffraction

CHAPTER ONE: INTRODUCTION

1.1 Overview

The development of porous ceramic materials has been a challenge to numerous industries because of the promising durability of porous ceramics in severe environments and their surface characteristics that makes them potential candidates for specific applications. With the growing demands of porous ceramics for industrial applications, a number of technologies have been developed to fabricate these materials with an attempt to control their pore characteristics. There has been a need for a thorough understanding of pore-related properties and thus to optimize the processing parameters.

Porous ceramic materials with more delicate and uniform pore structures and pore size ranging from a few hundred micrometers to a few nanometers can be achieved for diverse applications by either physical or chemical processing. The structure and properties of porous ceramics are found to be significantly controlled by their processing parameters. In the past decades, various processing routes had been proposed for the synthesis of porous ceramics, such as direct foaming of ceramic slurries of sol–gel solution [1, 2], chemical vapor deposition of various refractory materials on foamed carbon skeletons [3], sintering of hollow spheres [4],

replicating a polymer foam/sponge and mixing an organic or polymer powders/fibers with ceramic precursor [5]. Investigations on polymer-derived ceramics technique demonstrated that a controlled high surface area and uniformly distributed 3D ordered porous structure could be developed using controlled pyrolysis. The basic steps that are involved in producing PDPC are: (i) synthesis of polymer precursors, (ii) cross-linking the polymer to form pre-ceramic network, (iii) compounding the polymer precursors and additives to produce a foamable composition, (iv) decomposition of the pre-ceramic precursors and additives and creating numerous pores and (v) transforming the pre-ceramic network into porous ceramics.

Fabrication of the non-oxide porous ceramics via the method of PDC is a novel technique. Compared with conventional processes, porous ceramics can be prepared from a chemically stable precursor. In the meantime, the pore characteristics of the achieved porous ceramic can be easily tailored using different size and amount of sacrificial silica spheres. Furthermore, PDPC can be synthesized at a temperature as low as 1000 ^{o}C free of any additives, and cost-efficient manners which the powder-route can not perform.

In this thesis, the fundamental theories, fabrication techniques, characterization of porous ceramics and properties evaluation are clearly reported.

1.2 Objectives

The current work began with the investigation of the structure and properties of polymer-derived porous SiCN ceramics. Strong evidence indicates that the properties of the porous ceramics were directly related to its structure factors, i.e., the bulk density, open pore size, porosity and pore distribution. In order to obtain their ability to perform desired functions in a particular application, the objectives of my research mainly focused on two aspects. One is to fabricate the porous ceramic structure with controlled pore size and porosity. The other is to explore the effect of porosity/ pore size on properties such as permeability, mechanical behavior, high temperature oxidation, and thermal stability.

CHAPTER TWO: BACKGROUND

2.1 Properties and Applications of Porous Ceramic Materials

Although natural zeolite was discovered almost 250 years ago, it was only recently (1940s) that synthetic zeolite with excellent absorption properties was prepared. There is a great deal of incentive to develop large pore ordered porous materials because of many potential applications [6].

Porous ceramics possess a number of favorable properties which combine the merits of ceramics and porous materials such as light weight, low density, low thermal conductivity, low dielectric constant, thermal stability, high specific strength , high specific surface area , high porosity, high permeability, high wear resistance, and high resistance to chemical attack [7,8,9].

With these unique characteristics, the application fields of porous ceramics have been observed to significantly extend the range available to an engineer. The need for filtration of high temperature and pressure has lead to the development of porous ceramic filters that remove particles at efficiencies (in term of particle sizes removed per unit particle) higher

than cyclones, scrubbers, and electrostatic precipitators. Additional applications with similar requirements include recovery of methane from mines, removal of carbon dioxide and hydrogen sulfide from nature gas, and recovery of hydrogen in petroleum refinery operation. In the foundry industry, porous ceramics have been employed to filter for hot metal including super alloys: cast iron, steel, aluminum, and other nonferrous metals. These filters must withstand not only temperature but also resist attack by reactive elements that may rapidly degrade the ceramics [10, 11].

Another important application of porous ceramic is noted in support materials for advanced catalysts that can operate under harsh conditions due to their high thermal, mechanical, and chemical stabilities. Large surface area is required for good contact between catalyst and fluid stream as in catalyst support [10]. In particular, the catalyst supported porous materials have been successfully applied in the mass transfer of the catalytic combustion [12,13], combustion in situ in underground reservoirs for enhanced oil recovery [14], efficient heat transfer devices[15] and the reduction of hazardous combustion products [16].

In the biomedical field, advances in porous ceramics have led to their use as implant support materials. Bio-technology is using porous ceramics which can be made of phosphate ceramics such as hydroxyapatite, to simulate bone and some research has shown the porous ceramics with pore size larger than 100um can promote bone growth [17, 18, 19, 20].

The most well- known application of porous ceramics on the U.S Space Shuttle is the thermal protection materials. When the orbiting spacecraft and satellites are exposed to hypervelocity impacts against orbiting objects of various natures during reentry into the atmosphere, the porous ceramics represent a good candidate for the requirement of a reusable system to thermally protect the space shuttle [21, 22, 23, 24].

Additionally, porous ceramic are also used as chromatography [25], sensors [26], battery materials [27], and optic–electronic devices [28]. Recently they have been proposed as three-dimensional reinforcement in interpenetrating phase composites [29].

2.2 Processing Methods of Porous Ceramics

Porous ceramics are a specific class of porous material that consists of a three-dimensional array of polyhedral cells, packed to fill space and possessing a geometry that, when isotropic, can be approximated to that of a tetrakaidecahedron [30]. Porous materials have commonly divided into two categories, reticulated or open cells and closed cells, depending on whether cell faces are present. Cells can be surrounded by ceramic walls (randomly oriented in space) or the solid can be contained only in the cell edges (struts). In open cells both the pores are

three dimensionally interconnected, while in closed cell solids, the pores are isolated within the cells [31, 5]. Subsequently, the pore structure can be classified into four basic types: (1) fiber networks, (2) closed pore structures, (3) open pore structures, and (4) membranes [5].

The structure and properties of porous ceramics are controlled by their processing. Several processing routes for porous ceramics have been developed for specific applications as well as their associated requirements of porosity, pore size and degree of interconnectivity. Traditionally, porous ceramics have been produced by mixing ceramic powders with an organic material or calcium carbonate then formed into an appropriate shape. During the firing process, the organic materials burn away or the carbonate calcines giving off carbon monoxide gas leaving pores in the ceramic body. This processing method is commonly used to form high temperature ceramics with coarse pore size of 20-50um and has been used in the refractory industry for many years [5]. The other traditional method that has been studied since the 1960s uses the acid leaching of silica based systems to produce pores [32, 33]. With the extension of applications of porous ceramics, more and more techniques for processing the porous ceramics have been developed. Based on different pore structures, the main methods are summarized as following.

In the 1970's, a rigid fiber insulation (RSI) was developed with optimum thermal cycle tolerance. RSI is composed of blown high-silica fibers 1-3um in diameter with a colloidal

silica binder. The fibers are mixed in water slurry that gels, is formed into porous blocks, then is dried and sintered [5].

Closed cell ceramics are commonly formed by sintering hollow spheres. The technique is rather straightforward as it depends on sintering. If the green body is formed by pressing the spheres into a mold, it is critical to apply an appropriate amount of pressure so as not to crush the spheres [34, 35]. A novel approach to sintering hollow spheres developed by Meek, et al. [36, 37] involves the microwave heating of glass and metal micro-spheres. The micro-spheres or balloons range from 30 to 130um in diameter for glass and 400-600um for metal. Nakajima, et al. [38] produces a porous alumina by partially reacting coarse alumina powders with ultra fine silica powders. Mullite foams on the surface of the alumina during firing binding alumina particles together leaving pores. In this process, it is critical to not sinter at too high a temperature to avoid reduction in porosity.

A technique for production of partially closed cell ceramics by foaming a silica sol has been developed by Fujiu et al [39]. A colloidal silica sol is mixed with a surfactant, and methanol then liquid Freon is added as a foaming agent followed by quick gelation to fix the foamed structure. The foam is next dried then sintered.

Porous ceramics with an open cell structure are usually formed either by replicating a polymer foam/sponge or mixing polymer powder with the ceramics [40, 41]. Ceramics made by the polymer foam method are processed by one of three routes: (1) coating the foam with ceramic slurry and additives then sintering, (2) coating the foam with a sol-gel or colloidal solution followed by drying and sintering, or (3) pyrolyzing the polymer foam then coating the carbonaceous skeleton with ceramic using chemical vapor infiltration technique (CVI). For ceramics made by this method, there is either a hole or a carbonaceous material at the center of each strut due to the burn out of the polymer foam. The nature of this defect is critical to the mechanical properties of the porous ceramics [5].

Open cell ceramics made by coating polymer foams with ceramic slurry contain appropriately sized ceramic powders, sintering aid and binding agents. The resulting porous ceramic is very similar to the original polymer foam yielding pore size only slightly smaller than the foam and achieving porosities of approximately 70%. The coated foam is then heated to an appropriate sintering temperature. During heating, the polymer foam is burned leaving holes in the struts between pores [5].

The second way is to coat the polymer foam with either a sol-gel or colloidal solution [42, 43]. The Sol-Gel process is a chemical approach to allow synthesizing ceramic materials of high

purity and homogeneity by means of preparation techniques different from the traditional process of fusion of oxides. This process occurs in liquid solution of organic metallic precursors, which by means of hydrolysis and condensation reactions lead to the formation of a new phase (Sol). The Sol is made of solid particles of a diameter of few hundred of nm suspended in a liquid phase. Then the particles condense in a new phase (Gel) in which a solid macromolecule is immersed in a liquid phase (solvent). Drying the Gel by means of low temperature treatments (25-100 ℃), it is possible to obtain porous solid matrixes. Using the technique, pore diameters are less than 200um and there is a porosity of 97% with more fully open pores than achieved by the slurry coating technique. The sol-gel or colloidal solution is incorporated into the polymer exactly like water is soaked up into a sponge: the foam is compressed, immersed in the solution, and then allowed to expand to take in solution. After soaking in the solution, the coated foam is carefully compressed by rolling to remove excess solution then dried at room temperature.

The third technique of coating the polymer foam is to first pyrolyze thermosetting polymer foam to form a carbonaceous skeleton then coat it using chemical vapor infiltration (CVI) [44]. Typically, coatings of 10-1000um thick are deposited onto the surface of the foam and dominate the structure and properties of porous ceramics. The deposited layers are usually fully dense with grain size in the range of 1-5 um yielding mechanical strength up to twice that measured for ceramics foamed by slurry coated foam techniques.

Of the various methods used for ceramic membrane preparation the sol-gel technique is considered to be the most practical one because of its ability to make micro scale thin membranes having nano-scale pore diameters with a narrow pore size distribution. There are two types of sol-gel processing used, namely colloidal suspension and polymeric gel methods. Both methods utilize either metal salts or alkoxides as precursors [45, 46].

2.3 Polymer –derived Porous Ceramics

In this thesis, the main results concerning the highly porous ceramics from polymer-derived ceramics (PDC) will be discussed. Historically, the earliest report on the pyrolysis of silicones to obtain silicon-based materials was by Weyer [47]. As quoted by Rice [48], the comprehensive approach to obtain ceramics from polymer precursors was preformed at the British Ceramic Research Association under the guidance of Popper in the early 1960s. Despite some attempts to prepare SiCN and relative materials in the 1960s, the general potential of pre-ceramic compounds in the area of ceramics was not recognized until the pioneer work of Verbeek [49, 50] and Yajima [51,52] who prepared precursor-derived Si_3N_4 and SiC ceramic fibers. Since then the route of synthesizing Si/C/N ceramics from polymer precursors has attracted increasing attention, and a variety of new organ metallic polymers

have been developed as precursors for different non-oxide ceramics.

Three main ways of fabrication have been employed here for porous ceramics via PDC method: (1) direct foaming of a solution of a thermosetting silicone resin in a suitable solvent (with or without the addition of precursors), acting also as a blowing agent; (2) the use of sacrificial fillers that decompose during pyrolysis, consisting of polymeric micro-beads; and (3) the mixing of pre-ceramic polymers possessing different characteristics, in particular ceramic yield, depending on their molecular structure [53]. The first suggestion, which can be found in the patent literature, involves direct blowing [54, 55, 56] or by solvent extraction from a phase-separated polysilane gel [57]. The sacrificial template technique usually consists of the preparation of a composite comprising a matrix of ceramic particles and a dispersed sacrificial phase that is ultimately extracted to generate pores within the microstructure [58]. Moreover, recent papers have been published dealing with the preparation of meso-porous ceramics via self-assembly of a pre-ceramic polymer [59], via infiltration into meso-porous templates [60, 61], or via synthesis of an inorganic–organic diblock copolymer [62]. All these proposed processing methods allow producing ceramics with engineered porosity, affording varied and tailored characteristics that are of interest for a wide range of applications.

The process of the polymer-derived porous ceramic can be classified into seven stages: (i) synthesis of the liquid precursor; (ii) cross-linking of polysilazanes precursor into

pre-ceramic intermediate (infusible solids); (iii) milling the cross-linked silazanes into fine powders; (iv) mixing the pre-ceramic powders with a certain ratio of pore former powders; (v) shaping green bodies in different shape; (vi) decomposition of pore former and pre-ceramics intermediate which is achieved either thermally (pyrolysis, via conventional oven annealing, microwave or laser heating) or non-thermally (for instance by irradiation with ions) [53]; and (vii) structural rearrangement of the pre-ceramics intermediates to achieve the conversion of polymer to ceramics . The flow chart of the fabrication process is schematically represented in Figure 1. The unique feature of this novel process is the direct transformation from highly cross-linked polymer networks to porous Si/C/N bodies by pyrolysis without sintering aids. The details of this route will be introduced in the following sections.

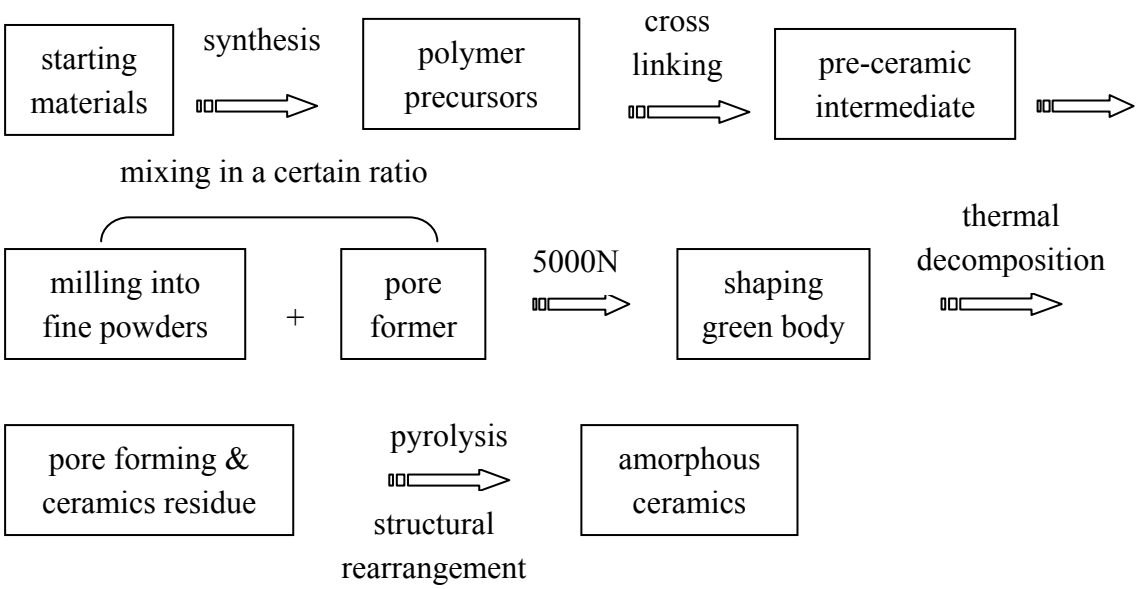

Figure 1 : The flow chart of fabrication of PDPC

2.3.1 Polymeric Precursors

Based on the work of Verbeek and Winter [63] as well as Yajima [64] in the 1970s, considerable interest was focused on the pyrolysis of pre-ceramic polymers. Hence, in the last decades a whole variety of such precursors were synthesized and the pyrolysis products were characterized.

In order to obtain any kind of ceramic materials from organic metallic compounds, the starting precursors have to be synthesized. Wynne and Rice [65] have set forth a series of general empirical rules that should be considered for the design of a proper ceramic precursor, and Seyferth [66] also stated various requirements for this purpose. Briot et al. stated a compromise of properties that an ideal pre-ceramic polymer should possess, which are sometimes incompatible:

1. Molecular weight should be sufficiently high to prevent any volatilization of oligomers
2. A polymeric structure should contain cages or rings to decrease the volatile fragments resulting from backbone cleavage
3. A polymeric structure should have desired viscoelastic properties (fusibility, malleability, or solubility) to apply the polymer in the desired shape before the pyrolytic process

4. A polymeric structure should present the latent reactivity (functional substituents) to obtain thermosetting or curing properties

5. Low organic group content should increase ceramic yield and avoid the production of undesired free carbon excess

It is evident that variations in functional substituent and different polymeric precursors' microstructures will strongly effect the final ceramic compositions and structures. Thus, a number of studies are devoted to the synthesis of pre-ceramic precursors and the subsequent precursors obtained upon judicious cross-linking. In this section, the polymer precursors of Si-C-N, and Si-Al-C-N will be mentioned.

2. 3.1.1 Polymeric Precursors of Si-C-N

Considerable effort has been put forth during the last few years to prepare ternary Si/C/N systems, and a wide range of polysilazanes oligomers bearing various adjacent hydrocarbon groups on silicon and nitrogen have been investigated as ceramic precursors. A commercially available product, KDT Ceraset Polysilazane 20 (VL20) owned by Kion Corporation is used as the polymeric precursor for preparation of SiCN/ SiAlCN ceramics. The VL20 is a versatile liquid thermosetting resin. This polymer contains repeat units in which silicon and

nitrogen atoms are bonded in an alternating sequence.

Its unit structure is described in Figure 2[67].

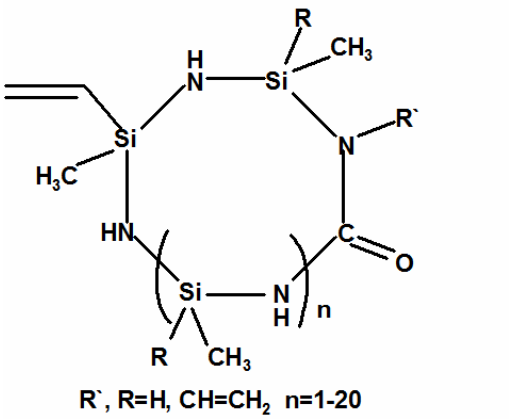

Figure 2 : The structure of liquid Ceraset Polysilazane 20

2.3.1.2 Polymeric Precursors of Si-Al-C-N

Multinary ceramics and composite materials are of interest due to their enhanced properties. For example, the addition of boron nitride leads to a better thermal shock resistance of hot-pressed silicon nitride ceramics [68]. Another promising element candidate is aluminum because AlN, Al_2O_3, SiAlON and other Al-containing materials show interesting properties such as high strength, high hardness or resistance to thermal shock and oxidation. In my work, the liquid Ceraset Polysilazane 20 with 10 wt% liquid aluminum sec-butoxide (Alfa Aesar,) is used as the polymeric precursor. The formation of polyaluminasilazane is the product from the dehydrocoupling reaction between the N-H bond in VL20 and Al-O bond in liquid

aluminum sec-butoxide. This reaction is accompanied by the evaporation of isopropoxide alcohol. The unit structure of polyaluminasilazane is presented in Figure 3.

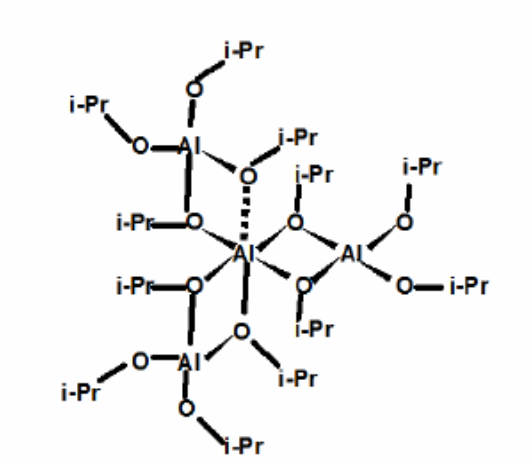

Figure 3 : The unit structure of polyaluminasilazane

2.3.2 Cross-linking of the Polymeric Precursors

The key steps to the PDPC process are the cross-linking process and the compaction process. Sevferth and Wiseman [69] have found that non-cross-linked precursors will cause lower ceramic yields (38%). The high degree of cross-linking is required in order to get a high-density final product. Cross-linking results in the oligomeric silazanes into large molecules with highly interlocked backbones, which are required to avoid the evaporation of oligomers during pyrolysis [70].

The effective cross-linking can be obtained by either thermally or chemically using radical

initiators like peroxides or catalysts. Thermal cross-linking is preferred on consideration of the control of elemental and phase composition of the final ceramics because no additional elements are introduced to the polymer. Thermal cross-linking requires the presence of reactive functional groups such as vinyl or silyl groups in the precursors. The major cross-linking reactions involved in the pyrolyzing polysilazanes are shown in Figure 4 [71, 72, 73, 74]. The VL20 solidifies mainly by the hydrosililylation reaction. Intense cross-linking results in a highly interconnected backbone structure that is infusible and easy to shape by powder processing.

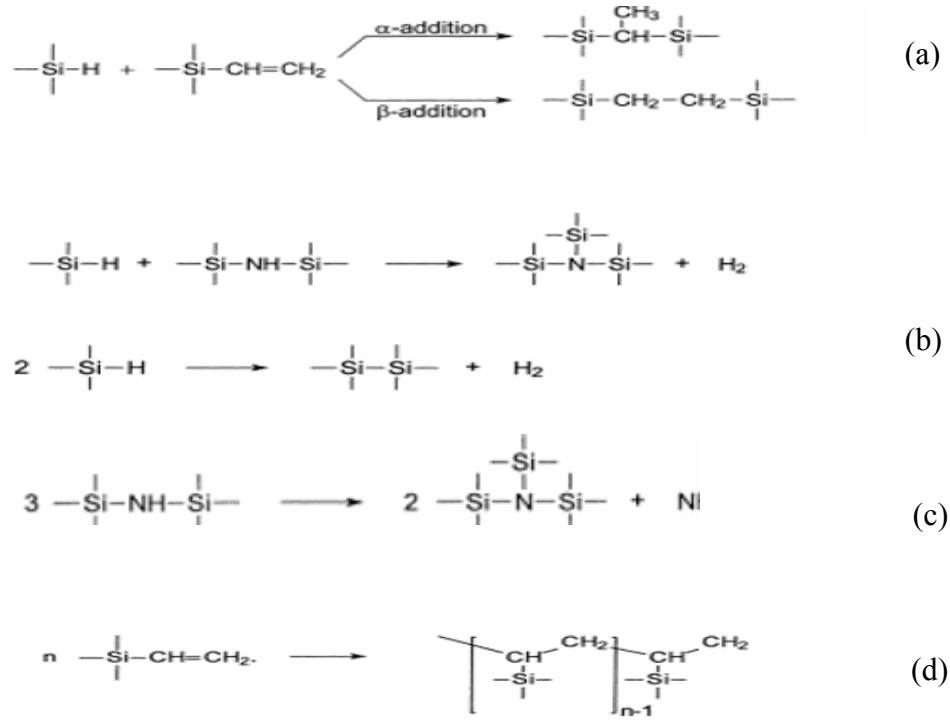

Figure 4: Cross-linking reactions in the pyrolyzing polysilazanes a) hydrosilylation of vinyl groups, b) dehydrocoupling of Si-H and N-H, c) transaminations by trisililating nitrogen atoms, and d) vinyl polymerization reaction.

2.3.3 Pore Former

An appropriate polymeric pore former must be selected. Two aspects are critical and need to be considered: one is the pore size, which determines the final pore size of the ceramic and second is the type of the polymer. Of the polymers available for pore formers, polyurethane (PU) is the most attractive because of its low softening temperature and ease of burn off which minimizes thermal stress that may fracture the unsintered ceramic [5]. A large and increasing number of original papers, as well as some review articles related to this topic are published each year. Recently, my research explored a new polymer pore former material, Polyvinyl Alcohol (PVA), which is similar to PU and quite suitable to fabricate porous ceramics. PVA has a relatively simple chemical structure with a pendant hydroxyl group. Its structure of PVA (partially hydrolyzed) is given as Figure 5[75]. It can be fully decomposed by breaking of C–H bonds, and release of H_2 and CH_4 and other volatile compounds at temperature (lower 400℃) before the pre-ceramic intermediate begins to decompose.

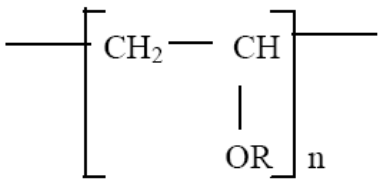

where R = H or $COCH_3$

Figure 5: The molecule structure of PVA

2.3.4 The Conversion Process to From Polymer to Ceramics

The conversion of the polymer into an amorphous ceramic material is a very complex process, especially for the correlation between the precursor architecture and the structure of the amorphous materials. The polymer-to-ceramic conversion is achieved either through pyrolysis (conventional oven annealing [76], microwave [77] or laser heating) or via non-thermally means (irradiation with ions [78]), usually including processing in controlled atmosphere [79]. Pre-ceramic polymers, organic-inorganic polymers whose backbone contains usually Si atoms, give a ceramic residue through the elimination of organic moieties [80, 81]. The ceramic yield of pre-ceramic intermediates strongly depends on their chemistry, including backbone structure and the functionality as well as the degree of cross-linking.

The weight loss during pyrolysis was caused predominately by the evolution of oligomers at lower temperatures and by-product gases at higher temperatures. A three-stage weight loss was generally observed for the polysilazanes [82]. First, weight loss occurred at temperatures lower than 400℃ due to the evaporation of light molecular weight oligomers and transamination reaction. There is also a contribution from hydrosilylation reaction in case of precursors with reactive groups of Si-H and $CH=CH_2$. The second weight loss comes from the loss of hydrocarbons such as CH_4, C_2H_6 and others in the temperature range of 400-750℃. Also, there is some dehydrogenative coupling with Si-H and N-H groups. Above 750℃, the weight loss is mainly due to hydrogen evolution. The exact temperatures of gas evaporation

change with the different polymer structure and the degree of cross-linking. There is also some variability due to the heating rate and pyrolysis environment.

During the pyrolysis process, the carbon in the polymer precursor will be redistributed. Some carbon turns into gas as hydrocarbons, some remains in the structure as free carbon which is present as basic structural units of carbon around the silicon network, and the remaining carbon is present in the silicon network environment of the amorphous structure SiC_xN_{4-x} [83]. The carbon in the structure can act as a diffusion barrier and prevents crystallization of stable phases such as SiC and Si_3N_4. As reported by many investigators [84, 85, 86, 87], the amorphous structure of SiCN consists of the mixed tetrahedra of SiC_4, SiC_3N, SiC_2N_2, $SiCN_3$, and SiN_4.

CHAPTER THREE: SYNTHSIS OF POLYMER-DERIVED POROUS SiCN/SiAlCN CERAMICS

In this chapter, I will systematically describe the synthesis process of polymer-derived porous SiCN/ SiAlCN ceramics and report the conventional parameters of these materials. In my present research, the conventional parameters are responded in terms of the measurements of the bulk density, open porosity, line shrinkage, morphology, pore size and permeability.

3.1 Synthesis of Porous SiCN/SiAlCN Ceramics

3.1.1 Fabrication of Pre-ceramic Intermediate

The liquid VL 20 is mixed with 5wt% thermal initiator, Dicumyl Peroxide (Acros Organics) and is continuously stirred until the thermal initiator is totally dissolved. The solution is solidified at 135ºC in vacuum and is further cross-linked at 350ºC for 3 hours in a nitrogen atmosphere to produce transparent polymer rods. Then the polymers are ball-milled for different times to get different size powder, which are called pre-ceramic intermediate powders.

For SiAlCN-10 ceramics, the liquid VL 20 with 10-wt% liquid aluminum sec-butoxide (Alfa Aesar,) is used as starting materials. They are mixed together and continuously stirred for several hours until aluminum isopropoxide is completely dissolved. Gaseous by-products are removed by placing the mixture in a vacuum before the thermal-setting step. This precursor is then mixed with 5wt% thermal initiator, dicumyl peroxide. The cross-linking and ball-milled processes are the same as that for the SiCN ceramics.

3.1.2 Fabrication of Porous SiCN/SiAlCN Ceramics

The powder of PVA with various particle sizes is uniformly blended with pre-ceramic intermediate powder in any certain ratio. In my work, the ratios of PVA to pre-ceramics we designed were 1:1, 2:1 and 4:1 and the particle sizes of PVA we selected were <106um, 106-212um and >212 um. The mixtures were put into a die with a diameter of one inch and then were compressed by applying a load of 5000N for 2 min. The shaped samples were placed in an aluminum boat and heated from the ambient temperature to 1000℃ in a tube furnace in the protection of nitrogen. The heating route was: room temperature ⟶ 200°C (5°C/min) ⟶ during 60min⟶400 °C (3°C/min) ⟶ during 90min ⟶1000°C (3°C/min) ⟶ during 120 min⟶ room temperature (8°C/min). After pyrolyzing the green body, we cured the samples at 800°C for ten hours in air to remove the free carbon existing in the samples.

3.2 Characterization of Porous SiCN Ceramics

3.2.1 Bulk Density and Open Porosity

3.2.1.1 Test Principle

For PDPC, its microstructure consists of a combination of open pores, closed pores and ceramic matrix. Here we use the bulk density and open porosity to present the structure's physical properties of porous SiCN ceramics. Bulk density is the mass of many particles of the materials divided by the volume they occupy. The volume includes the space between particles as well as the space inside the pores of individual particles [88].

The measurements of bulk density and open porosity are based on the Archimedes principle [89], as shown in Equations 3-1 and 3-2.

$$\rho = \frac{m_1}{V} \qquad V = \frac{m_2 - m_2'}{\rho_{H_2O}} \tag{3-1}$$

Where, ρ___ bulk density of the sample, g/cm^3.

m_1____initial weight of the sample measured in air, g.

V____ volume of sample including the solid and void, cm^3.

m_2____ sample weight after waterproof treatment measured in air, g.

m_2'_____ sample weight after waterproof treatment measured in water, g.

ρ_{H2O}___ density of water,g/cm^3. 0.9982 g/cm^3 at 20°C and .0.9957 g/cm^3 at 30°C.

Open porosity (ε) is a measurement of the void spaces in a material, which is the volume of open pore space (V_p) divided by the total volume of material *(V)*, including the solid and void components [89].

$$\varepsilon = \frac{V_p}{V} \times 100\% \qquad V_p = \frac{m_2 - m_1}{\rho_{oil}} \tag{3-2}$$

Where, ε____ volume fraction of open porosity of samples.

ρ_{oil} ____ density of oil, g/cm^3.

3.2.1.2 Test Equipments and Procedure

The equipment of measure weight is shown in Figure 6 and the vacuum equipment of filling oil is shown in Figure 7.

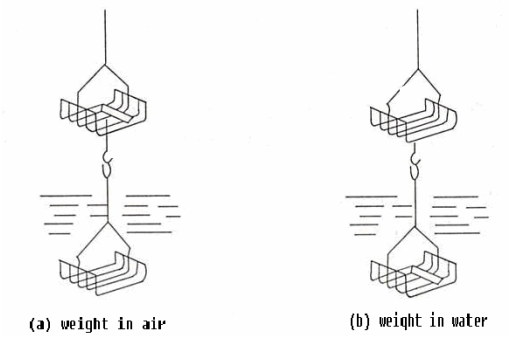

Figure 6 : The equipment for measuring weight

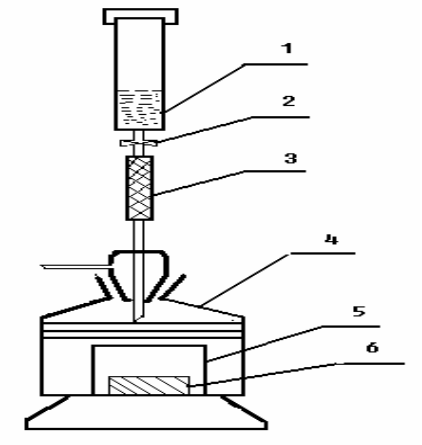

Figure 7: The vacuum equipment for filling oil，1，vessel filled with oil 2, valve 3, rubber vacuum tube 4, dryer vessel 5, beaker 6, sample

Procedure:

1) Clean and dry samples before testing.

2) Measure the initial weight of the samples in air, getting m_1.

3) Make samples vacuum, then pour oil into samples, keeping vacuum until no bubbles coming out form the surface of the samples.

4) Take the samples out quickly then remove the oil form the surface of samples, and measure the weight in air getting m_2.

5) Put the samples into water, then measure weight of sample in water getting m_2'.

6) We know the density of water and oil under test condition, using the Equation 3-1 and 3-2 to calculate the bulk density (ρ) and the open porosity (ε) of the samples.

3.2.1.3 Results and Discussion

The experimental results of the bulk density and open porosity of SiCN ceramics are listed in Table 1.

Table 1 : The Bulk Density and Open Porosity of SiCN Ceramics

PVA Size (um)	Ratio(PVA: Precursor)	Density (g/cm^3)	Porosity (%)
<106	1:1	0.75	60.0
	2:1	0.72	64.0
	4:1	0.56	71.8
106-212	1:1	0.66	67.0
	2:1	0.62	69.0
	4:1	0.60	70.0
>212	1:1	0.62	69.0
	2:1	0.58	71.0
	4:1	0.56	72.0

Discussion

The results show that both the ratio of PVA to pre-ceramic intermediate and the particle size of the PVA can effect directly on the final structure of the porous ceramic. More initial content of PVA and bigger sizes of PVA corresponded to lower bulk density and higher open porosity in ceramics. This is good certification for PVA decomposing completely in the pyrolyze process and leaving pore structure in the ceramic matrix.

3.2.2 Line Shrinkage

Shrinkage is a common phenomenon in the sintering process of polymer-to-ceramic conversion accompanied by significant weight loss and evolution of gaseous by-products. The shrinkage is caused by the necking and grain growth in the densification process. Therefore, the shrinkage is an important parameter which the engineers have to take into account for materials designed in the practice. Here, we employed the line shrinkage to present the shrinkage of porous SiCN ceramics.

The Line shrinkage (LS) of the samples after pyrolyzing at 1000℃ was calculated by using Equation 3-3 [23]. A vernier caliper was used to measure the dimensions of the specimen, before and after pyrolyzing, symbolized L_b and L_a, respectively. The results of measurement are shown in Table 2.

$$LS = 100 \times (\frac{L_b - L_a}{L_a}) \qquad (3\text{-}3)$$

Table 2 : The shrinkage of porous SiCN ceramics

Ratio(PVA: Precursor)	Shrinkage (%) with various PVA Size (um)		
	<106	106-212	>212
1:1	24.8	21.7	22.0
2:1	35.5	32.7	26.7
4:1	41.0	41.3	40.6

The data indicates that the increasing of concentration of PVA in raw materials will enhance the line shrinkages of the porous ceramics. The influence of the particle size of PVA is less effective in controlling shrinkage compared with the variation of the concentration of PVA.

3.2.3 Morphology of Porous SiCN Ceramics

Morphology is the study of the microstructure of materials, which characterizes the final property of the materials. Morphology of the porous ceramics is more complicate than that of bulk materials and therefore has more meanings for us to explore its details. The microstructure characterization of the pyrolyzed polymer-derived materials was performed by SEM, which is a powerful tool used to detect the morphology of the materials. The SEM pictures of porous SiCN ceramics are depicted in Figures 8 and 9.

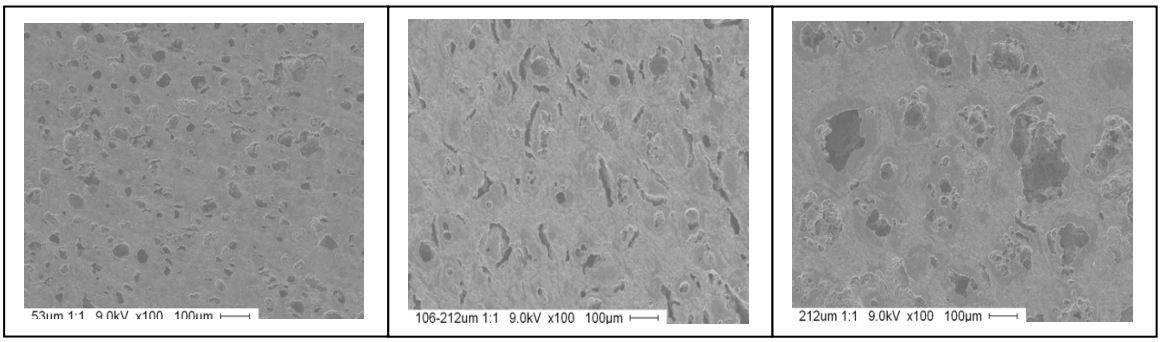

(a) (b) (c)

Figure 8: SEM pictures of porous SiCN ceramics with different size of PVA
53um PVA (b) 106-212um PVA (c) >212um PVA

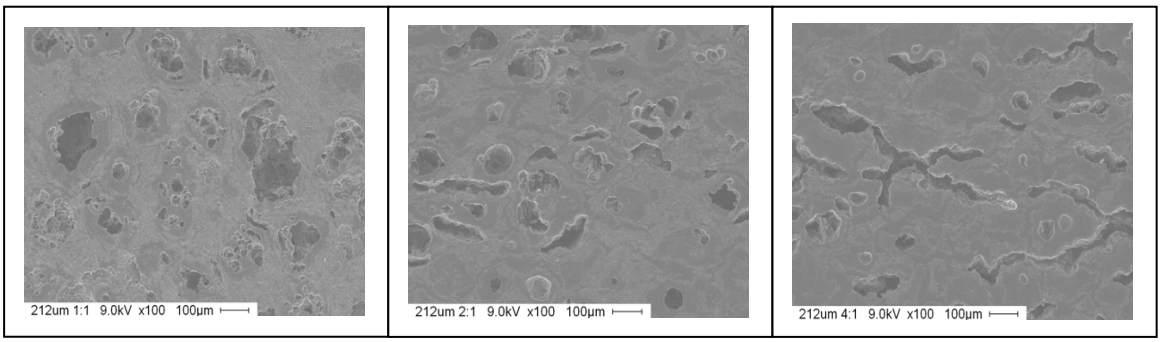

(a) (b) (c)

Figure 9: SEM pictures of porous SiCN ceramics with different ratio of PVA to precursor
(a) 1:1(b) 2:1 (c) 4:1

Discussion:

From these pictures, we can observe the porous SiCN ceramics' pore microstructure, including not only pore size and pore shape but also pore distribution and the pore connectivity in three dimensions. With the increasing size of the PVA, the shape and size of

pores change from regular small circles to irregular narrow strips to wider circles. Meantime, the percentage of the PVA in raw materials also influences the final size and distribution of pores, the more PVA, the larger pore area and the easier pore connectivity. These characterizations are very important for the industrial viability of this route.

3.2.4 Analysis of Pore Size of Porous SiCN Ceramics

3.2.4.1 Principle

Pore size of porous materials is an important parameter, especially for filter materials in the industry. Its measurement is determined by a non-destructive dynamic water-expulsion method [90, 91]. The method is based on the relationship between the pressure difference between the two ends of the samples and the flux of the gas through the porous materials. The corresponding pore size at each pressure gradient is calculated from the Washburn equation (3-4):

$$r=\frac{2\sigma\cos\theta}{\Delta P} \qquad (3\text{-}4)$$

Where, r —— radius of the pore, m.

θ —— contact angle between liquid and solid

σ —— surface tension coefficient, N/m. water is 0.07275 N/m.

ΔP —— the pressure difference between the two ends, Pa.

In its data computation, the pores are assumed to consist of many parallel, cylindrical capillary tubes and the Poiseuille's Equation 3-5 is applied to relate flow rate and pressure drop.

$$Q = n \times \frac{\pi}{8} \times \frac{\Delta P}{b \times l \times \eta} \times r^4 \qquad (3\text{-}5)$$

Here, Q —— the flux through the porous materials under the certain ΔP, m^3/s.

n —— the number of the pores with the same size

l —— the thickness of the samples, m.

b —— curve coefficient which is related to the ratio of the real path of the fluid passing to the thickness of the samples.

η —— dynamic fluid viscosity, $N.s/m^2$.

Simplify the Equation 3-5, $Q = K \times \Delta P$ (3-6)

K is a constant $$K = n \times \frac{\pi}{8} \times \frac{r^4}{b \times l \times \eta} \quad (3\text{-}7)$$

Prior to measurement, the samples are fully saturated with water. The numbers of the pores that gas can pass through increase gradually with the increase in the pressure difference (ΔP). The relationship between flux (Q) and the pressure difference can be determined by two factors: (1) the flux which is contributed by these pores that have already been opened, will be linear to the pressure difference, which means the flux increases with the increase in the pressure difference. (2) With the increasing in pressure difference, some new pores will be opened gradually. As a result, the flux caused by these new additive pores will not be linear to the pressure difference any more. All in all, the relationship between flux and the pressure difference will obey a curve showed in Figure 10. After all of the pores in the samples are open, the flux will be a line and determined by factor (1) [92, 93].

From the Figure 10, we can get the three points of pressure difference, ΔP_{min}, ΔP_{ave}, and ΔP_{max} respectively. ΔP_{min} is corresponding to the minimum pressure difference what we need to open the first biggest pore in the sample. ΔP_{max} is the transition point from curve to line, where the last pore in the sample will be opened, which means ΔP_{max} is the maximum pressure difference needed to open the last smallest pore in the sample. If we think the sample is consisted of many pores with same size, the size of the pore will be defined as the

average size of the pore. The ΔP_{ave} will be the pressure what we need to open these pores. Using the Equation 3-4, substituting the ΔP by ΔP_{min}, ΔP_{ave}, and ΔP_{max}, we can obtain the r_{max}, r_{ave} and r_{min} [92, 93].

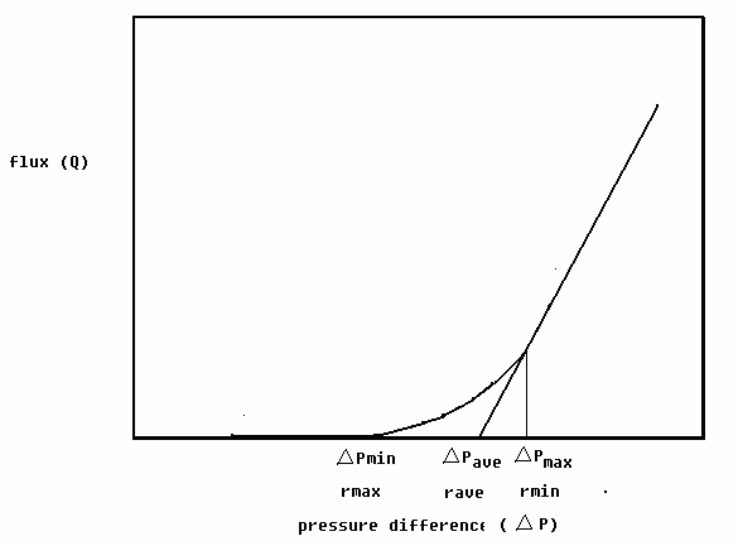

Figure 10 : Flux and the Pressure Difference Curve

3.2.4.2, Test Equipment

The equipment for measuring pore size is shown as Figure 11.

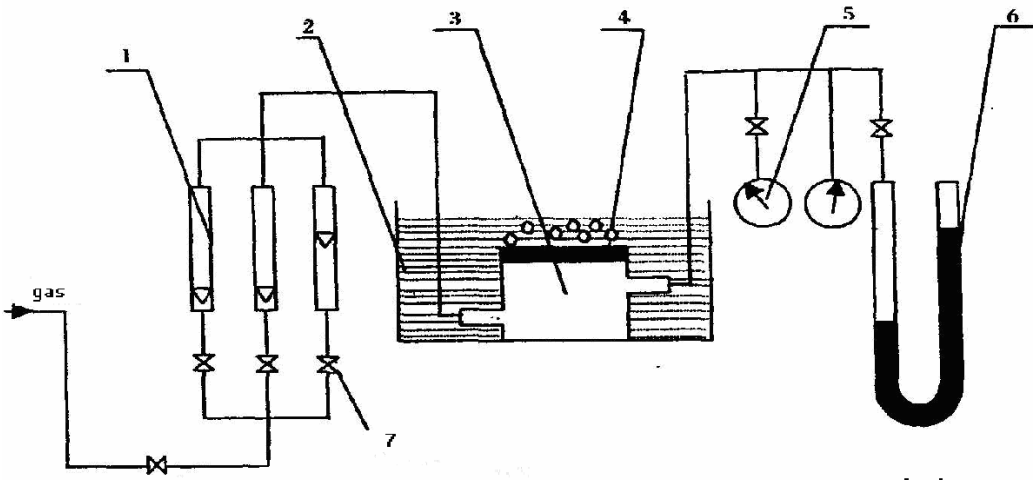

Figure 11: The equipment of measurement for pore size, 1, flow meter 2, water 3, sample chamber, 4, sample, 5, manometer 6, U-tube manometer 7, valve

We choose three different ranges of the flow meters to adjust the various samples. The chamber is used to fix the samples. It requires that the sample must be airproof by the gaskets. Manometer is used to measure the pressure difference between the two ends gas passing through the sample.

3.2.4.3, Test Procedure

1) The sample is exposed to a vacuum, and then the pure water is poured onto the sample so that the vacuum ensures that no bubbles come out from the sample and that it is immersed completely by pure water.

2) After fully wetting the sample with pure water, the sample is fixed on the chamber and

filled with pure water to the height of 3-6mm.

3) Open the switch of the gas, the gas reaches to the sample chamber via the flow meter. The velocity of the gas is controlled by the valve 1.

4) We can make the velocity of the gas very slow at the beginning until the first bubble comes out from the surface of the sample. We write down the ΔP which is in response to the maximum size of the pore.

5) Gradually increasing the gas flow, we can record the ΔP at each value of Q until we can see all pores in the sample begin to bubble and there is a linear relationship between the Q and the ΔP. Then plot the curve by the test points, and calculate the size of the pores.

3.2.4.4, Test Results and Discussion

Table 3 lists the results of the maximum, average and minimum pore sizes of porous SiCN ceramics.

Table 3: The pore size of porous SiCN ceramics

samples	Size of the pores (um)		
	r_{max}	r_{ave}	r_{min}
< 106 1:1	4.12	1.63	1.16
< 106 2:1	4.28	1.91	1.43
< 106 4:1	4.48	2.11	1.62
106-212 1:1	16.2	4.50	3.23
106-212 2:1	12.1	6.71	4.41
106-212 4:1	19.4	8.01	6.06
>212 1:1	45.5	13.3	10.0
>212 2:1	48.5	19.8	13.2
>212 4:1	52.9	20.8	14.6

Discussion

The pore size we measured via this method is representing the size of the entire open pores in the materials, which is consistent with the application of the porous materials in industry. The pore size is affected by many factors such as the irregular shape of the pores and the filter conditions. Generally speaking, if we use the size of pores to represent the size of the filtered particles, it will be 2.5 times of the size of the filtered particles. For the porous materials made by the non-circular particles, the size of the pores we obtained will even be 5 times of the size of the filtered particles. From the data, we can conclude that the pore size is increasing with the increasing of the size of the PVA and the percentage of PVA, which

means that we can get the final pore size what we desired by controlling the processing [92].

3.2.5 Analysis of Gas Permeability

3.2.5.1 Principle

Gas permeability (κ) can be defined as the ability of gas to pass through the porous materials under the driving force of the pressure difference. The gas permeability (κ) can be determined by measuring the gas pressure difference and the flux of the gas when the gas is passed through the porous sample [92].

By Darcy's Equation 3-8,

$$Q = \frac{-\kappa A \Delta P}{\mu L} \tag{3-8}$$

Where, Q____the total flux gas passing through the samples, L/ min •cm^2•Pa.

κ____the permeability of the medium, m^2.

A_____ the cross-sectional area to flow, m^2.

ΔP_____the pressure drop, Pa.

Ц_____dynamic viscosity, Pa·s.

L_____ the length the pressure drop is taking place over in sample, m.

3.2.5.2, Test Equipment and Procedure

The equipment for gas permeability of porous materials is described as in Figure 12.

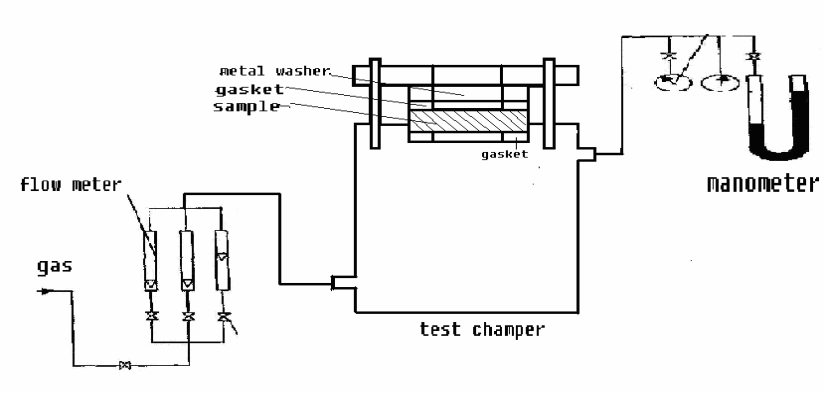

Figure 12 : The equipment for fluid permeability of porous materials

Procedure

1) Clean samples and measure its thickness and diameter before testing.

2) Fix the sample into the test chamber and make sure the sample is airproof.

3) Open the gas valve to make the value of the manometer 1000 Pa for a while, and then record the value of the flow meter.

4) Utilized the Equation 3-8 to calculate the permeability (κ)

3.2.5.3, Test Results and Discussion

Table 4 gives the measured and calculated parameters of samples prepared under different sizes and percentages of PVA.

Table 4 : The gas permeability of porous SiCN ceramics

samples	Flux Q (L/ min •cm^2•Pa)	Gas permeability **κ** (m^2)
< 106 1:1	6.35×10^{-5}	4.73×10^{-13}
< 106 2:1	2.11×10^{-5}	1.59×10^{-13}
< 106 4:1	2.47×10^{-5}	1.41×10^{-13}
106-212 1:1	2.97×10^{-4}	2.59×10^{-12}
106-212 2:1	1.19×10^{-4}	1.11×10^{-12}
106-212 4:1	8.24×10^{-4}	4.51×10^{-12}
>212 1:1	4.70×10^{-4}	3.84×10^{-12}
>212 2:1	9.59×10^{-4}	7.12×10^{-12}
>212 4:1	3.78×10^{-4}	2.22×10^{-12}

Discussion

In practice, the law regarding permeability is the bigger the value of the permeability, the better the permeability of the sample. As expected, the high porosity of the porous SiCN

ceramics yielded by the PDC method occupied the higher permeability. The permeability of porous materials only attributed to the existence of open-cell pores and closed-cell pores will not contribute to the permeability. From the data, we can make the conclusion that the influence of the size of PVA to permeability is greater than the influence of the concentration of PVA to the permeability. There are many factors which can affect the permeability in porous materials, mainly responding to the aspects of the pores' shape, size and distribution. The tendency is that with the increased porosity, the permeability will be enhanced.

CHAPTER FOUR: MECHANICAL BEHAVIOR OF POLYMER-DERIVED POROUS SiCN CERAMICS

The mechanical properties of a material determine its limitations for structural applications where the material is required to sustain a load. To make a judicious candidate material selection for the specific applications, it is useful to understand mechanical property theories and test. Theoretically, the effect on mechanical behavior of an internal pore would produce a much lower strength. It is necessary for us to know the mechanical behavior of the porous SiCN ceramics yield by PDC method in order to satisfy various needs in applications of industry [93]. In this thesis, the mechanical behavior of porous SiCN ceramics will be characterized by the fracture strength at room temperature, the fracture strength after thermal shock and the hertzian indentation strength.

4.1 Fracture Strength of PDPC at Room Temperature

4.1.1 Introduction

The strength of ceramic materials is generally characterized by bending testing (also referred to as flexure testing). The fracture strength in bending technique has been widely used to evaluate the mechanical properties of ceramic materials. The fracture strength is defined as

the maximum stress at failure. The test specimen is supported at the ends and the load is applied either at the center (three- point loading) or at two positions (four-point loading) and Figure 13 schematically illustrates the geometry of strength test.

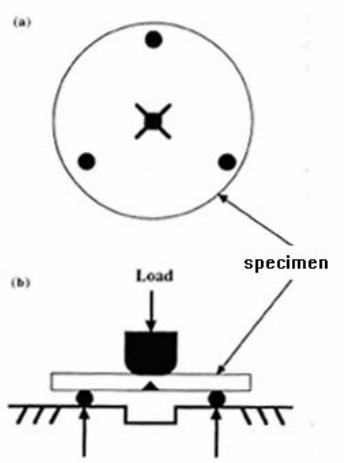

Figure 13 : Illustration of strength test: (a) bottom view showing the specimen geometry and (b) profile view showing the bottom support and the top punch.

The fracture strength σ can be calculated from the following Equations 4-1 to 4-3.

$$\sigma = -\left(\frac{3P}{4\pi \times t^2}\right)(X - Y) \qquad (4\text{-}1)$$

Where $$X = (1+v)\ln\left(\frac{R_L}{R}\right)^2 + \left(\frac{1-v}{2}\right)\left(\frac{R_L}{R}\right)^2 \qquad (4\text{-}2)$$

$$Y = (1+v)[1 + \ln\left(\frac{R_S}{R}\right)^2] + (1-v)\left(\frac{R_S}{R}\right)^2 \qquad (4\text{-}3)$$

R_L= radius of the region of the uniform loading = $(1.6\ z^2 + t^2)^{1/2}$- 0.675t (z is contact radius of the loading flat, 1.5 mm);

R_S = radius of support circle, 0.004m;

R = radius of specimen,

P = load at failure, N;

v = Poisson's ratio，0.3;

t = sample thickness, m.

The ratio of PVA to pre-ceramic intermediate in the specimen are 1:1, 2:1, and 4:1 with PVA having a particle size of 106-212um. For each group of samples, we did the three times of test in order to get the repeating results. The disk samples, after the pyrolyzing and heat treatment of the removal free carbon, were polished to 1um to make sure the surface was quite flat. Before the test, we measured the diameter and the thickness of the samples using a micrometer. The indented disks were broken in biaxial flexure using a three- point support and circular-flat loading fixture on a universal testing machine (model 3369, Instron Corp).

4.1.2 Results and Discussion

The experimental results of porous SiCN ceramics fracture strength at room temperature are shown in Table 5.

Table 5 : The fracture strength of porous SiCN ceramics

	No	Thickness (mm)	Diameter (mm)	Maximum Load (N)	Strength (MPa)
1:1	1	2.0	20.2	12.6	3.10
	2	1.7	20.1	10.31	3.52
	3	2.0	20.0	13.9	3.42
avg					3.08
2:1	4	1.9	18.2	4.19	1.15
	5	1.9	18.0	4.57	1.26
	6	1.9	18.1	4.83	1.33
avg					1.24
4:1	8	2.0	14.8	7.01	1.95
	9	1.9	14.8	4.96	1.95
	10	2.0	14.0	7.41	1.87
avg					1.93

From the experimental data, we can obtain the load-extension curves of each group of samples presented at Figure 14.

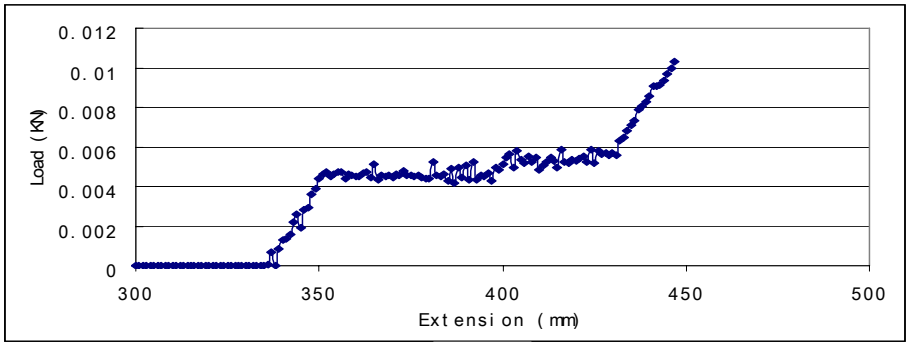

(a)

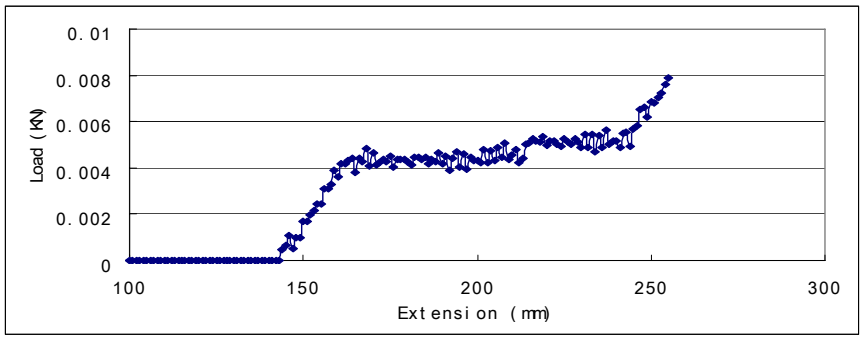

(b)

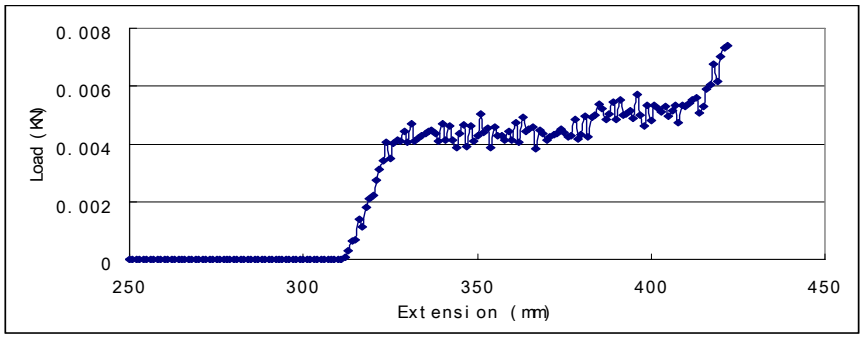

(c)

Figure 14: The Load-Extension Curve of Porous SiCN ceramic with different ratio of PVA to pre-ceramic intermediate, (a) 1:1, (b) 2:1, (c) 4:1

Discussion

The tendency to accurately describe the mechanical behavior of the porous ceramics materials is consistent with a number of empirical and semi –empirical models, which show the presence of porosity within a ceramic component and can be expected to lead to a reduction in flexural strength as a function of the porosity. One of the most commonly used forms of Equation 4-4 describes the effect of porosity on mechanical property as:

$$X = X_0 \exp(-bVf_P) \qquad (4\text{-}4)$$

Where X is the mechanical property, Vf_P is the volume fraction of porosity, b is an empirical constant and the subscript 0 indicates zero porosity. Equation 4-4 was originally proposed by Duckworth1 to describe the effect of porosity on strength following experimental work by Rysckewitch [94].

The effect of an internal pore on the fracture strength depends on many factors such as the shape and size of the pores, the distribution of pores and the distance between the pores [95]. A simple spherical pore theoretically would have less stress concentration effect than a sharp crack. However, the pores in ceramics are not perfectly spherical. Some are roughly spherical but most are highly irregular. From the morphology of SEM pictures, we can see that the samples with a ratio of 1:1 have more regular circle shape and the samples with ratio of 2:1 and 4:1 will become sharper and irregular [95]. Most experimental data are able to render the

pore size effect on strengthening for relatively large pores leading to lower strengthening. In the meantime, the reduction in strength with increased amounts of discrete non-homogenous pores is frequently greater than that predicted by models based on a homogenous pore distribution [96]. The reason is because the pore coalescenceleads to a larger defect size, resulting in a lower strength [97].

From the above points, all factors result to the strength of samples with 1:1, 2:1, and 4:1 will degrade gradually, however, there is an uncommon result in samples of 2:1 and 4:1. In my opinion, the reason to explain this result is that the distance between the pores plays an important role in the fracture process of materials. By the morphology pictures I mentioned in chapter 3, the pores cluster in the samples with the ratio of 4:1 is more severe than that of the samples with the ratio of 2:1. This means the distance among pores in samples of ratio of 4:1 is relatively larger than the distance of the pores in samples of ratio of 2:1. The thicker wall of the pores will be beneficial to contribute the larger fracture strength [98].

The mechanical behavior of porous materials shows failure modes such as buckling and bending of the struts under the application of an external load. When a porous material is compressed, the force vs. displacement curve shows three regions [99]. Initially the struts begin to deform in a linear-elastic manner; then a plateau occurs where the porous material is completely crushed and finally there is a region of densification as the cell walls crush

together. The extent of each region depends on the relative density of the porous material. Elastic porous material, plastic porous material and brittle porous material all have the three parts in their force-displacement curve, but the mechanism causing the plateau is different in each case. The plateau is associated with collapse of the cells. In elastic porous materials (rubbers), collapse is accompanied by the elastic buckling of the cell walls; in materials with a plastic yield point (metals) it occurs by the formation of plastic hinges at the maximum load; and in brittle material such as ceramics it is caused by brittle fracture of the struts [100].

4.2 Thermal Shock Effects on the Strength of PDPC

4.2.1 Introduction

Thermal shock occurs when a thermal gradient causes different parts of an object to expand by different amounts. This differential expansion can be understood in terms of stress or of strain, equivalently. At some point, this stress overcomes the strength of the material, causing a crack to form. If nothing stops this crack from propagating through the material, it will cause the object's structure to fail [95].

A simple thermal shock test has been devised via water-quench method. All specimens used in this experiment were the same as the samples described in 4.1 with the ratio of 1:1. The

effect of porous SiCN ceramics on the resistance to crack propagation during thermal shock was examined by subjecting samples to rapid changes in temperature by ice water quenching from 700 □, 900□, 1000 □and 1100□, respectively. Prior to quenching, samples were heated to the desired temperature and held for 30 min to ensure thermal homogeneity; then they were immersed immediately and simultaneously into the ice water bath. Following quenching, the samples were dried thoroughly prior to mechanical testing as described in section 4.1.

4.2.2 Results and Discussion

The experiment and calculation results are listed in table 6. The relationship between fracture strength and temperature change (ΔT) is shown in Figure 15.

Table 6 : The strength of porous SiCN ceramics after thermal shock

Temperature (℃)	No	Maximum Load P (N)	Fracture Strength (MPa)
700	1	10.54	2.88
	2	15.429	4.21
	3	14.006	3.82
AVG			3.66
900	1	6.727	3.37
	2	7.845	5.29
	3	13.89	3.42
AVG			4.03
1000	1	17.17	4.23
	2	34.02	6.27
	3	42.06	4.71
AVG			5.07
1100	1	31.53	7.76
	2	64.49	6.69
AVG			7.23

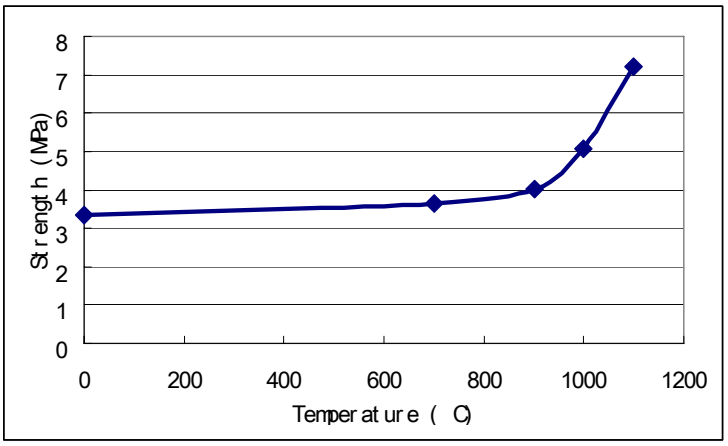

Figure 15 : Effect of thermal shock on strength of porous SiCN ceramics

Discussion

For most ceramics, the thermal shock is expected to be a problem, while from the experimental data, it clearly shows the polymer-derived porous SiCN ceramics behave as an excellent thermal shock resistance. With the increasing of ΔT, the bending strength is enhanced. Especially at ΔT more than 900 □, the difference of the strength is more dramatic. These improvements can be attributed to the pores in the specimens which relax the thermal shock stress and arrest the propagation of micro cracks effectively.

4.3 Hertzian Indentation Strength of PDPC

Porous SiCN ceramics with high porosity have been considered as one of the most favorable candidates for hot gas filtration in diesel exhaust systems. In these applications, the surfaces of porous SiCN ceramics are subjected to the continuous impact of solid particles. This may lead to localized damage and consequently to strength degradation or ultimately to catastrophic failure. Therefore, it is necessary to investigate the contact damage behavior of porous SiCN ceramics. As an effective technique under laboratory conditions, Hertzian indentation has been used to explore the contact damage in a variety of porous ceramics [101].

4.3.1 Principle

Hertzian indentation was first applied to investigate the contact behavior between two brittle specimens as early as 1881. The first experimental were conducted on two curved bodies. The most widely used configuration of the Hertzian test today is shown in Figure 16, where a rigid sphere is loaded onto a flat surface of test material. One advantage of Hertzian indentation, which renders it useful for the evaluation of contact deformation, is that the indentation pressure increases monotonically with load from first contact to the onset of first plastic deformation. The relationship between elastic strain and stress can be described by using the famous Hertzian contact Equation 4-6, where the radius of the contact circles a, is related to the indentation load P, the indenter radius R, and the elastic properties of the indenter and materials [102]:

$$P_m = \frac{3E_m}{4\pi \times k}(\frac{a}{R}) \tag{4-6}$$

Where $Pm=P/\pi a^2$ is the mean pressure of indentation and k is an elastic mismatch coefficient:

$$k = \frac{9}{16}[(1-v_m{}^2) + \frac{E_m}{E_S}(1-v_S{}^2) \tag{4-7}$$

Where E_m, v_m, E_s, v_s are the Young's modulus and Possion's ratio for the test material and the indenter respectively. Hertzian indentation is of great interest to materials scientists because of the fact that the elastic field, although complex, is well defined up to the point of fracture.

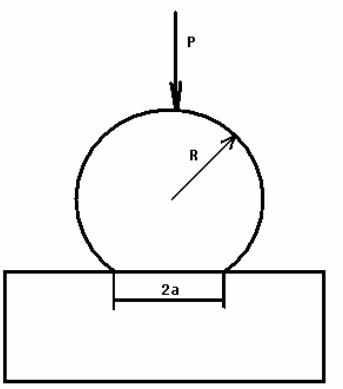

Figure 16 : Experimental geometry for measuring indentation stress-strain curve. Sphere of radius delivered load P over contact radius a

4.3.2 Experimental Procedure

In this experiment, we investigate the effect of different percentage and particle size of PVA on the surface damage of porous SiCN ceramics. In order to easily compare, we selected five typical groups of samples which are <106 um 1:1, <106 um 2:1, <106 um 4:1, 106-212 um 2:1, >212 um 2:1, respectively. Disk samples were ground and polished to 1um. These samples were then uniformly coated with a thin layer of carbon. Normally, Hertzian indentation tests were performed in air with a universal testing machine at a constant cross-head speed of 0.1 mm/min over a load range of 0–2000 N, using tungsten carbide spheres of radius R=12.7 mm as an indenter. Based on the measurements of contact of radii a from the residual impressions on the surfaces of the samples, the relative indentation strain (a/R) and the mean indentation stress ($P/\pi a^2$) can be calculated and the mean indentation stress ($P/\pi a^2$) can be described as a function of indentation strain (a/R).

4.3.3 Results and Discussion

The experimental results of the indentation strength of porous SiCN ceramic with various pore size and percentage of PVA are presented in Figure 17 and Figure 18, respectively.

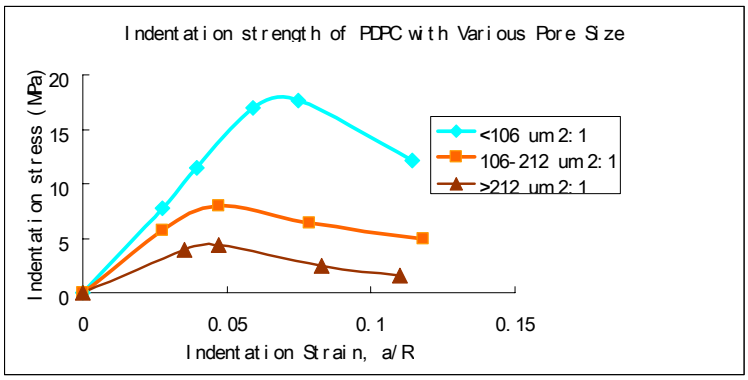

Figure 17：Indentation strength of SiCN ceramics with various particle sizes of PVA

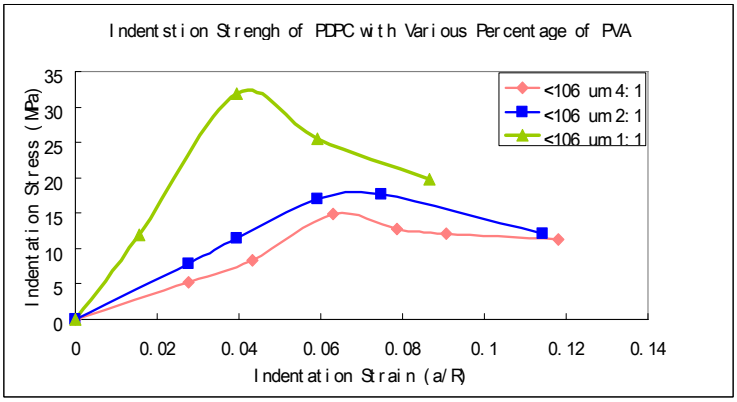

Figure 18：Indentation strength of SiCN ceramics with various percentages of PVA

Discussion

For most single-crystal and polycrystalline ceramics fracture in a brittle mode, there is no plastic deformation. However, from the Figures 17 and 18, the Hertzian indentation surface damage curve was observed both in an ideally elastic stress–strain response and a high ‘‘plasticity’’ deformation which deviates distinctly from Hertzian elastic response. By comparing the slope of the ideally elastic region, we can distinguish the Young’s modulus of the different groups of samples which responses the ability elastic deformation of the materials. It was found that the yield strength of porous SiCN ceramics will be enhanced with the decreasing of the porosity. This indicates that porosity may play a critical role in the contact damage process. However, the specific mechanisms of Hertzian contact damage in porous ceramics are not well understood.

CHAPTER FIVE: OXIDATION BEHAVIOR OF POLYMER-DERIVED POROUS SiAlCN CERAMICS

As research in the field of porous ceramic composites continues to expand, there is an increasing emphasis on the study and improvement of porous ceramics with some additives for the reinforcement of these materials. For example, a small mount of Al in ceramic composites can be capable of maintaining high oxidation resistance at high temperatures. The aim of this chapter is to study the oxidation behaviors of porous SiAlCN ceramics in a low temperature region (Oxide scales are amorphous). In this case, the oxidation kinetics is determined by measuring the change in weight of the samples as a function of the time at a certain temperature.

5.1 Oxidation Behavior of Silicon-based Materials.

Before discussing the oxidation of SiAlCN ceramics, it is appropriate to review the oxidation of pure silicon, for it sets a basis for all silicon-based ceramics. The classic paper in this area was written by Deal and Grove[103]. In this paper, it was assumed that oxidation proceeded by inward movement of oxidant rather than outward movement of silicon in accordance with the experimental evidence for silicon [104, 105, 106]. They viewed the oxidation process as consisting

of three distinct steps, as shown in Figure 19:

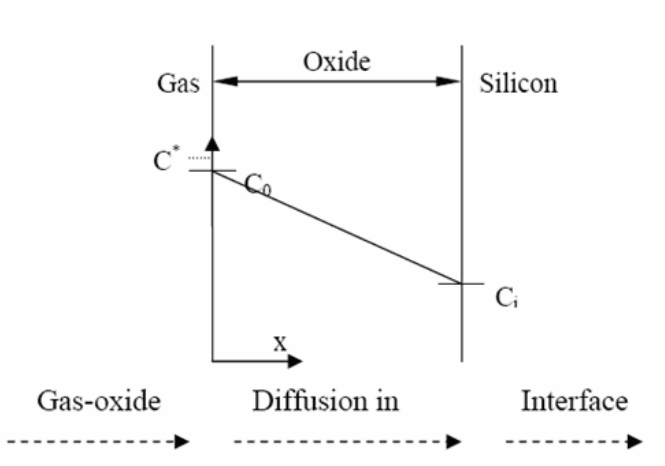

Figure 19 : Process involved in Silicon oxidation

1. Transfer of the gaseous oxidant to the outer surface where it reacts or is absorbed.

2. Transport of oxidant across the oxide film towards the silicon.

3. React at the silicon surface to form a new layer of SiO_2.

The oxidation behaviors of SiC and Si_3N_4 are more complex. In both ceramics, there is a countercurrent gas. The following reactions (Equation 5-1 to Equation 5-3) are generally accepted [107]:

$$SiC(s)+1.5O_2(g)=SiO_2(s)+CO(g) \quad (5\text{-}1)$$

$$Si_3N_4+0.75O_2(g)=1.5Si_2N_2O(s)+0.5N_2(g) \quad (5\text{-}2)$$

$$Si_2N_2O(s)+1.5O_2(g)=2SiO_2(s)+N_2(g) \quad (5\text{-}3)$$

Therefore oxidation process for SiC and Si_3N_4 involves five steps:

1. Transport of molecular oxygen gas to the oxide surface

2. Diffusion of oxygen through the oxide film

3. Reaction at the oxide/ceramic interface

4. Transport of product gases (e. g. CO or nitrogen)

5. Transport of product gases away from the surface

5.2 Experimental Procedure

The porous SiAlCN specimens are used in the oxidation experiments. The procedure for preparing these specimens was described in section 3.1.1. In order to entirely explore the oxidation behavior of porous SiAlCN ceramics, we selected the four groups of the samples which are <106 um 1:1, <106 um 2:1, 106 -212 um 1:1, and > 212 um 1:1, respectively.

Before oxidation, the samples were treated at 1300℃ for 4 hours to stabilize the structure. After heat-treatment, we measure the initial mass of each sample. The oxidation process is carried out in the air at 1000℃ and 1200℃ for 2, 4, 8, 15, 30, 60, 150, and 300 hours in the high-temperature tube furnace.

For oxidation at temperatures equal to or less than 1200℃, the SiAlCN samples are loaded in a high purity quartz tube. The oxidation experiments are carried out in an auto-programmable thermolyne alumina tube furnace (Barnsted/Thermolyne, Texas). The quartz tube is used to avoid any contamination from the alumina working tube. The furnace was then programmed to reach the desired temperature with a rate of 5 ^{o}C/min and is held there for a certain time. Then we cooled the samples to room temperature at a rate of 7 ^{o}C/min. We can obtain a relationship between the weight change and oxidation time at a specific temperature by measure the change of the mass of the samples at each stage.

5.3. Results and Discussion

In porous materials, the oxidation behavior can only be measured by the weight change of the samples. Figure 20 and Figure 21 plot the weight change of the oxide scales as a function of annealing time for the SiAlCN ceramics at 1000 ^{o}C and 1200 ^{o}C, respectively.

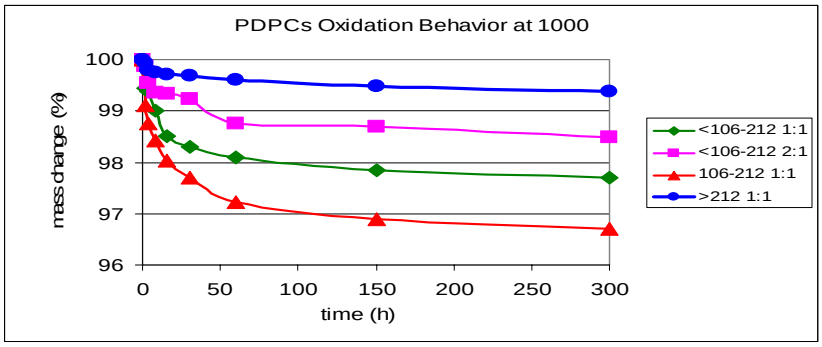

Figure 20 : Weight change of porous SiAlCN ceramics at 1000 ℃ with time

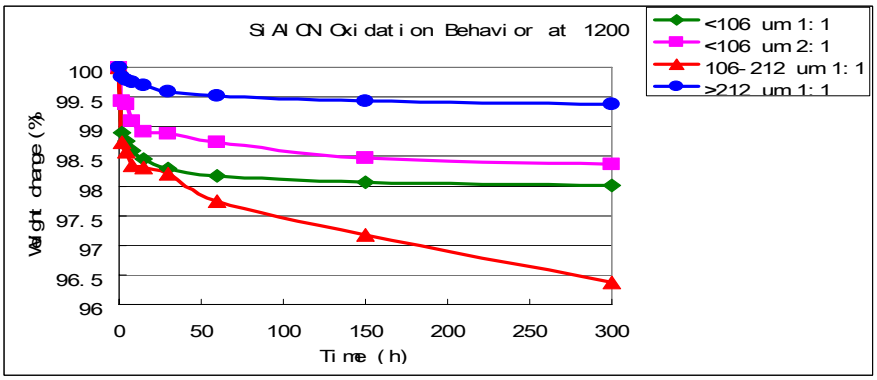

Figure 21 : Weight change of porous SiAlCN ceramics at 1200℃ with time

Discussion

The experimental data show that all samples exhibit weight loss at oxidation time up to 300 hrs at 1000℃and 1200℃. The weight loss of the samples may be caused by a small amount of decomposition of SiAlCN or the remains of free carbon in samples reacting with oxygen and releasing gas out.

During the entire heating process, the porous SiAlCN ceramics took place the oxidation reactions accompanied by the decomposition reactions. Form the decrease of the total weight of the samples, we can know the decomposition reactions are dominated and the decomposing rate is faster than the rate of the oxidation reactions.

CHAPTER SIX: THERMAL STABLILITY OF POLYMER-DERIVED POROUS SiAlCN CERAMICS

6.1 Introduction

The objective of our work was to determine the feasibility of maintaining thermal stability properties after exposure to high temperatures by applying nitrogen pressures while the porous SiAlCN ceramics is heated. The term thermal stability is defined by the resistance to permanent change in properties caused solely by heat. When applied to ceramics, it usually refers to their ability to withstand prolonged exposure to high temperatures, without a major change in their fundamental properties.

Some of the phenomena taking place are common in porous ceramic materials. Thus, the surface area decrease is related to processes which are favored by high temperatures, such as sintering and changes in the crystalline or non-crystalline phase. Other factors can accelerate the loss of surface area, as are the case of the reaction atmosphere (e.g. water vapor) and the composition of the solid phase (e.g. presence of alkaline compounds) [114].

There are several studies on the thermal stability of the porous ceramics, and nearly all of

them have been focused on thin film membranes. M.H. Jaskowiak found the polymer-derived porous SiC ceramics are thermally unstable beyond 1200 °C. These instabilities are believed to be caused by increased porosity and the growth of flaws which are initially produced during fiber fabrication. Outside the literature, it is worth mentioning the relatively few studies dealing with the stability of porous ceramics and the effect of additives such as alkaline-earth and rare earth compounds. In our research, the thermal stability was studied by the weight change as a function of temperature and microstructure analysis using X-ray diffraction (XRD).

6.2 Experimental Method

Polymer-derived porous SiAlCN ceramics were studied in this work. The preparation and selection of the samples were the same as the samples in the oxidation experiment mentioned in chapter 5.

The equipment of heat treatments for samples is performed by hot isostatic pressing (HIP) furnace. Samples were placed in a clean tungsten cup covered with a loose lid and loaded in a tungsten lined resistance heated furnace. To evaluate the long term effect of the N_2 treatments, samples were held at temperature and pressure for 4 hr durations. The specimen was exposed

to nitrogen gas at temperatures 1100 °C, 1200 °C and 1300 °C. In order to understand the effects of nitrogen exposure on polymer-derived porous SiAlCN ceramics' stability, these samples were weighed before and immediately after each heat treatment to obtain weight loss measurements at room temperature. X-ray diffraction of crushed samples was used to qualitatively evaluate the extent of microstructure growth of the porous SiAlCN before and after heat-treatment at each stage.

6.3 Results and Discussion

The weight change of each group of sample with various heat treatment temperatures under HIP condition in N_2 protection for 4 hours is plotted at the Figure 23.

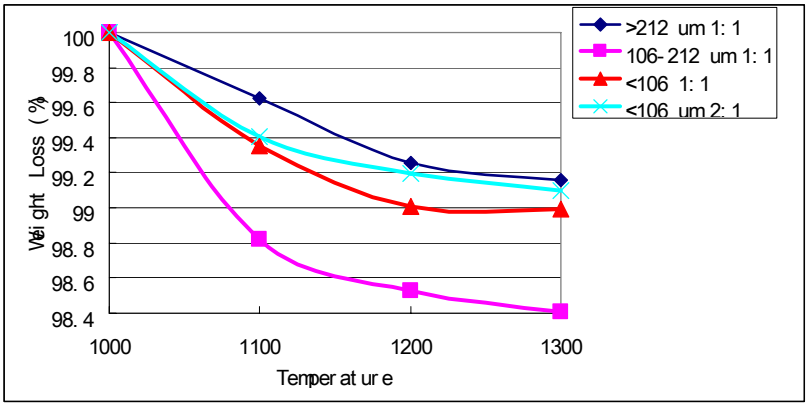

Figure 22 : Curve of weight loss of porous SiAlCN versus various temperatures at HIP condition

The x-ray diffraction results at each temperature are showed in the Figures 24, 25 and 26.

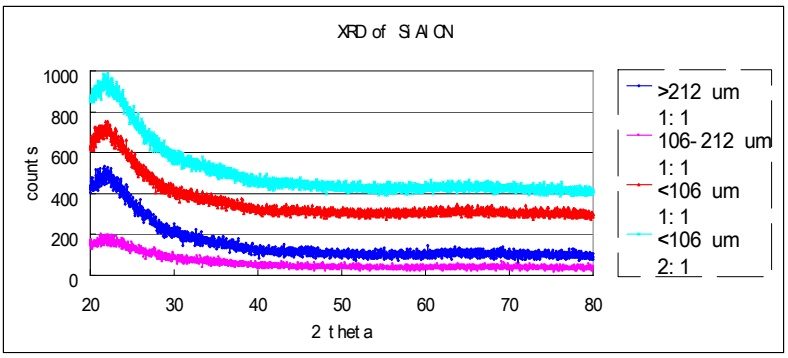

Figure 23 : XRD of SiAlCN under 1100 ℃ HIP treatment

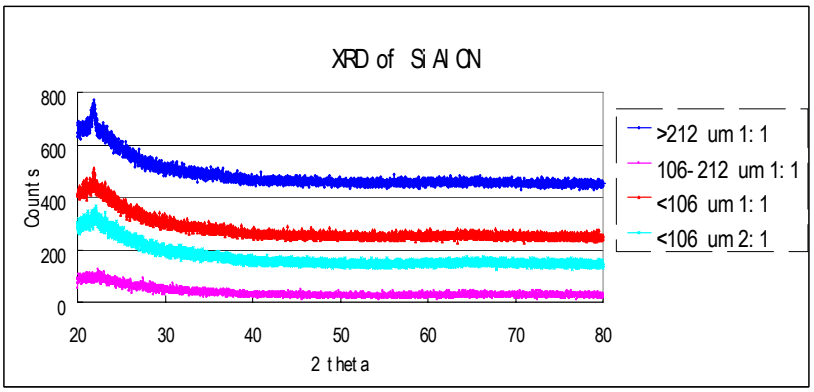

Figure 24 : XRD of SiAlCN under 1200 ℃ HIP treatment

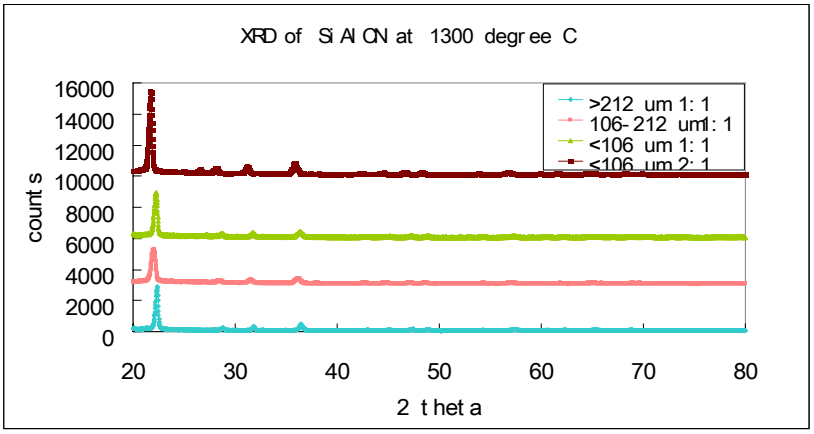

Figure 25 : XRD of SiAlCN under 1300 ℃ HIP treatment

Discussion

From the weight loss curves with various temperatures, we have observed a HIP nitrogen treatments limited weight loss to 2 percent or less for temperatures up to 1300 °C, which is exhibiting a high degree of thermal stability in these materials.

The x-ray diffraction patterns in Figures 24 and 25 display no distinct peaks forming and no indication of local nucleation or crystallization for the porous SiAlCN ceramics at 1100°C and 1200°C, respectively. They remained predominantly amorphous microstructure, therefore are stable against diversification within this temperatures range.

The crystalline phases were identified by X-ray diffraction (Figure 26). The diffraction

pattern clearly exhibits the presence of Si_3N_4 in the samples annealed above 1300 ℃. The crystallization strongly depends on the polymer architecture and on the residual porosity of the system. Their presence is not related to the short-range rearrangement occurring within the amorphous ceramics, but is a result of gas-phase reactions. The porous materials crystallized at relatively lower temperature as compared to their fully dense counterparts

CHAPTER SEVEN: CONCLUSION

In this work, it clearly demonstrated that the polymer-derived ceramics method can be used to synthesize porous SiCN/SiAlCN ceramics by using low molecular weight precursor and pore former. This is a remarkable achievement in the field of porous non-oxide materials. This novel process compared to the conventional method for the production of porous SiCN ceramics are: offering substantial flexibility in producing porous ceramics with tailored microstructure and properties, low processing temperature of about 1000℃, densification without sintering aids, low-cost and high efficiency. From the aforementioned discussion, the following conclusions can be drawn:

The amount of PVA and the particle size of PVA play an important role in the processing of porous SiCN ceramics. The pore parameters and properties can be easily controlled by varying the PVA concentration and the particle size.

This processing route enables the production of porous SiCN ceramics with lower bulk density 0.56-0.75 g/cm^3 (fully dense is about 2 g/cm^3) and higher open porosity up to 72%. The line shrinkage percentage of porous SiCN ceramics is ranged from 20% to 40% and the effect of the amount of PVA on shrinkage is more than the influence of the particle size on the shrinkage. Also the morphology of pore structure whatever the pore size and pore shape

will be changed by the variation of the compositions of raw materials.

As expected, the pore size and permeability of the porous SiCN ceramics measured by the method of water expulsion varied as a function of the content of PVA and the particle size of PVA. The pore size ranging in a very wide range of values (1-53um) and a higher permeability can be obtained.

It is known that the mechanical strength of the porous SiCN ceramics is affected by their porosity, and we can observe strength of the material synthesized in this work decrease with increasing porosity. It was found that the fracture strength of the porous SiCN ceramics based three-point bending test is ranging from 1Mpa to 3Mpa. Dramatic improvement of fracture strength was achieved after thermal shock at the temperature change more than 900℃. We investigated Hertzian indentation to measure surface stresses on porous SiCN ceramics. The present results show that the yield strength is also affected by the porosity and there is a reverse relationship between them.

Polymer-derived porous SiAlCN ceramics exhibit weight loss at oxidation time up to 300 hrs at 1000℃and 1200℃. The weight loss is due to the burn-out of pyrolysis residuals.

One of the key merits when employing newly developed polymer-derived porous SiAlCN

ceramics is their stability at high temperatures, in particular, the stability of the amorphous state. The weight change of porous SiAlCN ceramics under HIP condition is less than 2% of the initial weight when the temperature is up to 1300℃ for 4 hours and they remain predominantly amorphous before 1300℃.

LIST OF REFERENCES

[1] L.M. Sheppard, *Ceram. Trans*. 31, 3 (1993).

[2] P. Sepulveda and J.G.P. Binner, J. Euro. *Ceram. Soc*. 19, 2059 (1999).

[3] H. Hagiwara and D.J. Green, J. *Amer. Ceram. Soc*. 70, 811 (1987).

[4] K. Ishizaki, S. Komarneni, and M. Nanko, *Porous Materials*:Process Technology and Applications (Kluwer Academic, Dordrecht, The Netherlands, 1998), p. 181.

[5] D. A. Hirschfeld, T. K. Li, and D. M. Liu, *Key Engineering Materials*,Vol 115 (1996) pp 65-80.

[6] J. Weitkamp, *Solid State Ionics* 131, 175 (2000).

[7] C. W. J. Wang, C. B. Park, *Journal of Material Science* **39** (2004) 4913 – 4915.

[8] Gibson LJ, Ashby MF (1999) Cellular solids,*Sstructure and Properties,* 2nd edn. Cambridge University Press, UK.

[9] Colombo P (2002) Key Eng Mater 1913:206–213.

[10] L.M. Shepard "Corrosion Resistant Ceramics for Severe Environments," *Am. Ceram. Soc*. Bulletin 70[7], 1146-1158 (1991).

[11] J. F. Zievers, P. Eggerstedt, and E. C. Zievers, "Porous Ceramics for Gas Filtration", *Am. Ceram. Soc*. Bulletin 70[1], 108-111 (1990).

[12] M.W. Ryoo, S.G. Chung, J.H. Kim, Y.S. Song, G. Seo, *Catal. Today* 83 (2003) 131.

[13] T. Sano, H. Hagimoto, S. Sumiya, Y. Naito, Y. Oumi, T. Uozumi, K. Soga, *Microporous*

Mesoporus Mater. 44–45 (2001) 557.

[14] B.S. Gottfried, *Combust*. Flame 12 (1968) 5.

[15] S.B. Sathe, M.R. Kulkarni, R.E. Peck, T.W. Tong, An experimental and theoretical study of porous radiant burner performance, in: Proceedings of the Twenty-Third International Symposium on Combustion, 1991, pp. 1011–1018.

[16] B.H. Chao, H. Wang, P. Cheng, Int. J. Heat Mass Transfer 39 (1996) 3003.

[17] S.B. Bhaduri, *Advan. Perform. Mater*. 1, 205 (1994).

[18] L.M. Sheppard, *Ceram*. Trans. 31, 3 (1993).

[19] P. Sepulveda and J.G.P. Binner, *J. Euro. Ceram. Soc.* 19, 2059 (1999).

[20] C. Lavernia and J.M. Schoenung, "Calcium Phosphate Ceramics as Bone Subsititutes," *Am. Ceram. Soc*. Bulletin 70[7], 95-100 (1990).

[21]L. J. Korb, C. A. Morant, R. M. Calland and C. S. Thatcher, " The Shuttle Orbiter Thermal Protection System," *Am. Ceram. Soc*. Bulletin 60[11], 1188-1193(1981).

[22] D. B. Leiser, M. Smith, and H. E. Goldstein, " Developments in Fiberous Refractory Composite Insulation", *Am. Ceram. Soc*. Bulletin 60[11], 1201-1204(1981).

[23] J. D. Buckley, G. Strouhal, and J. J. Gangler, "Early Development Ceramic Fiber Insulation for Space Shuttle", *Am. Ceram. Soc*. Bulletin 60[11], 1196-1200(1981).

[24] J. Dumoulin, " Thermal Protection System" NASA World Wide Web, http://www.nasa.gov/shuttle/technology, 1994.

[25] R.A. Caruso, M. Antonietti, *Adv. Funct. Mater*. 12 (2002) 307.

[26] K.M. Kulinowski, P. Jiang, H. Vaswani, V.L. Colvin, *Adv. Mater*. 12 (2000) 833.

[27] H. Yan, C.F. Blanford, B.T. Holland, W.H. Smyrl, A. *Stein, Chem. Mater*. 12 (2000) 1134.

[28] P.D. Yang, A.H. Rizvi, B. Messer, B.F. Chmelka, G.M. Whitesides, G. Stucky, *Adv. Mater*. 13 (2001) 427.

[29] T.J. Fitzgerald and A. Mortensen, *J. Mater. Sci.* **30**, 1025 (1995) and *J. Mater. Sci*. 30, 1037 (1995).

[30] Gibson LJ, Ashby MF (1999) Cellular solids, *Structure and Properties*, 2nd edn. Cambridge University Press, UK.

[31] Saggio-Woyansky J, Scott CE, Minnear WP (1992) Bull *Am Ceram Soc* 71:1674

[32] M. B. Volf, *Technical Glasses*, Pitman, London, (1961).

[33] A. Makishima, J. D. Mackensie, J. J. Hammel, "The Leaching of Phase-Separated Sodium Borosilicate Glasses," *J. Non-Cryst. Solids*, 31,377-83(1979).

[34] A.Briggs, Energy Ceramics, Processings of the 4th International Meeting on Modern Ceramic Technologies, P. Vincenzi, ed, Elsevier Scientific Publishing Co, New York, 1980.

[35] D. J. Green, "Fabrication and Mechanical Properties of Lightweight Ceramics Produced by Sintering Hollow Spheres", *J. Am. Ceram Soc*, 68[7]403-9(1988).

[36] L. Saggio-Woyansky, C. E. Scott, and W.P. Minnear, "Processing of Porous Ceramics", *Am. Ceram Soc* Bulletin, 71[11], 1674-1682(1992).

[37] T. Meek, R.Blake, and T. Gregory, " Low Density Inorganic Foams Fabricated Using Microwaves", *Cream Eng. Sci Proc*, 6[7-8] 1161-70 (1985).

[38] H. Nakijima, T.Ito, and Y. Muragachi, "Alumina Porous Body and Production of the Same," U.S. Patent 4,965,230, Oct 23,1990.

[39] T. Fujiu, G. Messing, and W. Huebner, "Processing and Properties of Cellular Silica Synthesized by Foaming Sol-Gel," *J. Am. Ceram Soc*, 73[1]85-90(1990).

[40] K. Schwartzwalder and A. V. Somers, "Method of Making Porous Ceramic Articles," U. S. Patent No. 3, 090, 094, May 21, 1963.

[41] F. F. Lange and K. T. Miller, "Open-Cell Low Density Creamics Fabricated from Reiculated Polymer Substrates", *Adv. Cream. Mat*, 2[4], 827-31(1987)

[42] J. J. Brown, D.A. Hirschfeild, T. K. Li, "Alkalai Corrosion Resistant Coating and Ceramics Foam Having a Superfine Cell Structure and Method of Processing," *U. S. Patent* 5,268,199, Dec 7, 1993.

[43] T. K. Li, D.A. Hirschfeild, J. J. Brown, Unpublished Work, Virginia Polytechnic Institute & State University, 1992.

[44] R. H. Tuffias, and R. B. Kaplan, " Refractory Ceramic Foams: A Novel, New High Temperature Structure," *Am. Ceram. Soc*. Bulletin, 70[6]1025-1029(1992).

[45] L. C. Klein and N. Giszpene, *Am. Ceram. Soc*. Bulletin, 69[11]1821-25(1990).

[46] A. J. Burggraaf and K. Keizer, and R. R. Bhave, ed, Van Nostrand Reinhold, New York, 1991.

[47] D.F. Weyer, "Method of Preparing Ceramic Like Articles," *US Patent* 3,090,691, (1963).

[48] R.W. Rice, K.J. Wynne, and W. B. Fox, "Preparation of Ceramics," *US Patent* 4,097,294

(1978).

[49] W. Verbeek and G. Winter, "Silicon Carbide Fibers," *German Patent* 2,236,078 (1974).

[50] W. Verbeek, G. Winter, and M. Mansmann, "Molded Bodies of Homogeneous Mixtures of Silicon Carbide and Silicon Nitride," *German Patent* 2,243,527 (1974).

[51] S. Yajima, J. Hayashi, M. Omori, and K. Okamura, "Development of A Silicon-Carbide Fiber With High-Tensile Strength," *Nature* 261, 683-685 (1976).

[52] S. Yajima, K. Okamura, J. Hayashi, and M. Omori, "Synthesis of Continuous SiC Fibers with High-Tensile Strength," *J. Amer. Ceram. Soc*. *59*, 324-327 (1976).

[53] Paolo Colombo, "Engineering porosity in polymer-derived ceramics", *Journal of the European Ceramic Society* xxx (2008) xxx–xxx.

[54] Renlund, G. M., Minnear, W. P. and Bracco, A. A., Cellular silicon-oxycarbide glass from foamed silicone resins, *US Patent* 4,981,820, January 11991.

[55] Renlund, G. M., Lewis, L. N., Stein, J. and Bracco, A. A., Silicon-oxycarbide glass method of preparation and articles, *US Patent* 5,180,694, January 19 1993.

[56]Daws, D. E., Castellucci, N. T., Carpenter,H.W. and Colby,M.W., Methods for producing ceramic foams using pre-ceramic resins combined with liquid phenolic resin, *US Patent* 5,643,512, July 1 1997.

[57]Whinnery, L. L., Nichols, M. C., Wheeler, D. R. and Loy, D. A., Process for preparing silicon carbide foam, *US Patent* 5,668,188, September 16 1997.

[58] Jung-Hye Eom, Young-Wook Kim, In-Hyuck Song, Hai-Doo Kim, "Processing and

properties of polysiloxane-derived porous silicon carbide ceramics using hollow microspheres as templates" *Journal of the European Ceramic Society* 28 (2008) 1029–1035.

[59] Malenfant, P. R. L.,Wan, J., Taylor, S. T. and Manoharan, M., Self-assembly of an organic–inorganic block copolymer for nano-ordered ceramics. *Nat. Nanotechnol*., 2007, 2, 43–46.

[60] Yan. J. Wang, A. and Kim, D. P., Preparation of ordered mesoporous SiC from preceramic polymer templated by nanoporous silica. *J. Phys. Chem. B*, 2006, 110, 5429–5433.

[61] Krawiec, P., Geiger, D. and Kaskel, S., Ordered mesoporous silicon carbide (OM-SiC) via polymer precursor nanocasting. *Chem. Commun.*, 2006, 23, 2469–2470.

[62] Nghiem, Q. D., Kim, D. and Kim, D. P., "Synthesis of inorganic–organic diblock copolymers as a precursor of ordered mesoporous SICN ceramic". *Adv. Mater.*, 2007, 19, 2351–2354.

[63] Verbeek, W. and Winter, G., *O.enlegungsschrift* 2236078, 1974.

[64] Yajima, S., Okamura, K., Hayashi, J. and Omori, M., Synthesis of continuous SiC ®bres with high tensile strength. *J. Am. Ceram. Soc*., 1976, 59, 324±327.

[65] K.J. Wynne and R.W. Rice, "Ceramics via Polymer Pyrolysis," *Annu. Rev. Mater*. Sci. 14, 297-334 (1984)

[66] D. Seyferth, In Inorganic and Organometallic Polymers, edited by M. Zeldin, K.J Wynne, H.R. and Allcock. ACS Symposium Series 360, *American Chemical Society*, Washington DC,

1988

[67] http://www.ceraset.com/

[68] K.S. Mazdiyasni and R. Ruh, "High-low Modulus Si_3N_4-BN Composite for Improved Electrical and Thermal-shock Behaviors," *J. Am. Ceram. Soc. 64*, 415-419(1981)

[69] D. Seyferth, and G.H. Wiseman, "Polysilazane Routes to Silicon Nitride,"" *Polym. Prepr.* 25, 10-12(1984).

[70] D. Seyferth, in: *Euro-Ceramics* 2, Vol. 1, edited by G. Ziegler and H. Hausner, Deutsche Keramische Gesellschaft e. V.,Augsburg, 1991.

[71] C.K. Narula, Ceramic Precursor Technology and its Applications, *Marcel Dekker*, New York, 1995.

[72] N.S. C.K. Yive, R.J.P. Corriu, D. Leclerq, P.H. Mutin, and A. Vioux, "Silicon Carbonitride from Polymeric Precursors-Thermal Cross-linking and Pyrolysis of Oligosilazane Model Compounds," *Chem. Mater. 4,* 141-146(1992).

[73] D. Seyferth, in: Silicon Based Polymer Science-A Comprehensive Resource, edited by J.M. Ziegler and F.W.G. Feason, *American Chemical Society*, Washington, DC, 1990.

[74] M. Peuckert, T. Vaahs, and M. Bruck, "Ceramics from Organometallic Polymers," *Adv. Mater. 2,* 398-404 (1990).

[75] S.K.Saxena, "Polyvinyl Alcohol (PVA)", *Chemical and Technical Assessment,* 61st JECFA

[76] Monthioux M, Delverdier O (1996) *J Europ Ceram Soc* 16:721.

[77] Danko GA, Silberglitt R, Colombo P, Pippel E, *Woltersdorf J (2000) J Amer Ceram Soc*

83:1617.

[78] Pivin JC, Colombo P, Soraru GD (2000) J Amer Ceram Soc 83:713.

[79] Jacubenas K, Marcus HL (1995) J Am Ceram Soc 78:2263.

[80] Riedel R (1996) Materials science and technology, a comprehensive treatment. In: Brook RJ (ed) Processing of ceramics. *VCH, Wurzburg*, Germany, 17B[2]:1–50.

[81] Bouillon E, Langlais F, Piller R, Naslain R, Cruege F, Huong PV, Sarthou JC, Delpuech A, Laffon C, Lagarde P, Monthioux M, *Oberlin A (1991) J Mater Sci* 26:1333.

[82] N.S. Choong, R.J.P. Corriu, D. Leclercq, P.H. Mutin, and A. Vioux, "Thermogravimetric Analysis/Mass Spectrometry Investigation of the thermal Conversion of Organosilicon Precursors into Ceramics under Argon and Ammonia," *Chemistry of Materials, 4*, 1263-71 (1992)

[83] C. Haluschka, H.J. Kleebe, R. Franke, and R. Riedel, "Silicon Carbonitride Ceramics Derived from Polysilazanes Part I. Investigation of Compositional and Structural Properties," *J. Euro. Ceram. Soc. 20*, 1355-64 (2000).

[84] R. Riedel, H.J. Kleee, H. Schbrifelder, and F. Aldinger, " A covalent Micro/ Nano Composite Resistant to High temperature Oxidation*," Nature, 374*, 526-28 (1995).

[85] D. Bahloul, M. Pereira, and P. Goursat, "Silicon Carbonitride Derived from an Organometallic Precursor: Influence of the Microstructure on Oxidation Behavior," *Ceram. Int. 18*, 1-9(1992).

[86] G. Ziegler, H.J. Kleebe, G. Motz, H. Muller, S. Trapl, and W. Weibelzahl, "Synthesis, Microstructure and Properties of SiCN Ceramics Prepared from Tailored Polymers," *Mater. Chem. Phys. 61*, 55-63 (1999).

[87] H.J Kleebe, D. Suttor, and G. Ziegler, "Microstructure Evolution and Crystallization Behavior of Polymer-Derived Si-C-N Monoliths: A TEM study," *in Polymer Derived Ceramics,* edited J. Bill, F. Wakai, and F. Aldinger, Wiley-VCH Verlag byGmbh, Weinheim, Germany, 1999.

[88] http://en.wikipedia.org/wiki/Bulk_density

[89] "Sintered metal materials, excluding hardmetals -- Permeable sintered metal materials -- Determination of density, oil content and open porosity" *ISO 2738*:1999.

[90] *ASTM*, Standard test method for pore size characteristics of membrane filter with aerospace fluids, F316-80, vol 10.05, 1984.

[91] C. Gelinas and R. Angers, Improvement of the dymanic water-expulsion method for pore size distribution measurement, *Am. Cer. Soc. Bill.*, 65[9], 1297-1300,1986.

[92] Y. Wei, "Simplified analysis method of determining pore sizes of porous materials by bubble test", *Powder Metallurgy Industry,* Vol No.6 Dec. 2004.

[93] *ISO* 4003-1977 (E). "Permeable Sintered Metal Materials-Determination of bubble test pore size".

[94] Ryshkewitch, E., Compression strength of porous sinteredalumina andzirconia . *J. Am. Ceram. Soc.*, 1953, 36, 65–68.

[95] D.W. Richerson, "Modern Ceramic Engineering Properties, Processing, and Use in Design", Third Edition.

[96] R.A. Dorey1, J.A. Yeomans*, P.A. Smith, "Effect of pore clustering on the mechanical properties of ceramics," *Journal of the European Ceramic Society* 22 (2002) 403–409

[97] Jung-Hye Eom, Young-Wook Kim, In-Hyuck Song, Hai-Doo Kim, "Processing and properties of polysiloxane-derived porous silicon carbide ceramics using hollow microspheres as templates," *Journal of the European Ceramic Society* 28 (2008) 1029–1035.

[98] R.A. Dorey1, J.A. Yeomans, P.A. Smith, "Effect of pore clustering on the mechanical properties of ceramics", *Journal of the European Ceramic Society 22* (2002) 403–409

[99] F.M. Ashby, Metall. Trans. A **14**, 1755 (1983).

[100] L.J. Gibson and M.F. Ashby, Cellular Solids Structure and Properties (Pergamon Press, NY, 1988), p. 120.

[101] J. H. She, J. F. Yang, Y. Beppu, T. Ohji,"Hertzian contact damage in a highly porous silicon nitride ceramic" , *Journal of the European Ceramic Society* 23 (2003) 1193–1197.

[102] L.N. An, "Fracture and Contact Damage Behavior of Alumina-based Ceramic Composites", Dissertation, 1996.

[103] B.E. Deal and A.S. Grove, "General Relationship for the Thermal Oxidation of Silicon," *J. App. Phys. 36*, 3770-3778 (1965).

[104] J. R. Ligenza and W. G. Spitzer, "The Mechanisms for Silicon Oxidation in Steam and Oxygen," *J. Phys. Chem. Solids 14*, 131-136(1960).

[105] P. J. Jorgensen, "Effect of an Electric Field on Silicon Oxidation," *J. Chem. Phys. 37,* 874-877(1962).

[106] W.A. Pliskin and R. P. Gnall, "Evidence for Oxidation Growth at the Oxide-silicon Interface from Controlled Etch Studies," *J. Electrochem. Soc. 111*, 872-873(1964).

[107] N.S. Jacobson, "Corrosion of Silicon-Based Ceramics in Combustion Environments," *J. Am. Ceram. Soc. 76*, 3-28 (1993).

[108] R.E. Tressler, "Theory and Experiment in Corrosion of Advanced Ceramics,"pp3-22 in *Corrosion of Advanced Ceramics.* Edited by K.G. Nickel, 1994.

[109] T. Bakos, S.N. Rashkeev and S.T. Pantelides, "Reactions and Diffusion of Water and Oxygen Molecules in Amorphous SiO2," *Phys. Rev. Lett. 88*, 055508 (2002).

[110] S.V. King, "Ring Configurations in a Random Network Model of Vitreous Silica," *Nature 213,* 1112-3 (1967).

[111] P. Umari and A. Pasquarello, "Modeling of the Raman Spectrum of Vitreous Silica: Concentration of Small Ring Structures," *Physica B. 316-317,* 572-574 (2002).

[112] J.P. Rino, I. Ebbsjö, R.K. Kalia, A. Nakano and P. Vashishta, "Structure of Rings in Vitreous SiO_2," *Phys. Rev. B 47*, 3053-3062 (1993).

[113] K. Vollmayr, W. Kob and K. Binder, "Cooling-rate Effects in Amorphous Silica: A Computer-simulation Study," *Phys. Rev. B 54*, 15808-15827 (1996).

[114] D. Lafarga, A. Lafuente, M. Meneandez, J. Santamaroa, "Thermal stability of g-Al2O3/a-Al2O3 mesoporous membranes" *Journal of Membrane Science 147* (1998)

173±185